land

MDPI

Article

Spatially Explicit Model for Assessing the Impacts of Groundwater Protection Measures in the Vicinity of the Hranice Abyss

Jozef Sedláček [1,*], Hana Vavrouchová [2], Kryštof Chytrý [3], Ondřej Ulrich [2], Petra Oppeltová [2], Milan Geršl [4], Kristýna Kohoutková [1], Radim Klepárník [1], Petr Kučera [1], Vítězslav Vlček [5], Jana Šimečková [5] and Eva Žallmannová [1]

[1] Department of Landscape Planning, Faculty of Horticulture, Mendel University in Brno, 613 00 Brno, Czech Republic; kristyna.kohoutkova@mendelu.cz (K.K.); radim.kleparnik@mendelu.cz (R.K.); petr.kucera@mendelu.cz (P.K.); eva.zallmannova@gmail.com (E.Ž.)
[2] Department of Applied and Landscape Ecology, Faculty of AgriScience, Mendel University in Brno, 613 00 Brno, Czech Republic; hana.vavrouchova@mendelu.cz (H.V.); ondrej.ulrich@mendelu.cz (O.U.); petra.oppeltova@mendelu.cz (P.O.)
[3] Department of Conservation Biology, University of Vienna, 1090 Vienna, Austria; krystof.chytry@univie.ac.at
[4] Department of Agricultural, Food and Environmental Engineering, Faculty of AgriScience, Mendel University in Brno, 613 00 Brno, Czech Republic; milan.gersl@mendelu.cz
[5] Department of Agrochemistry, Soil Science, Microbiology and Plant Nutrition, Faculty of AgriScience, Mendel University in Brno, 613 00 Brno, Czech Republic; vitezslav.vlcek@mendelu.cz (V.V.); jana.simeckova.uapmv@mendelu.cz (J.Š.)
* Correspondence: jozef.sedlacek@mendelu.cz; Tel.: +420-731753325

Abstract: This study introduces a novel spatially explicit modeling framework developed to quantify the secondary environmental benefits of groundwater protection strategies in karst landscapes, with a specific application to the Hranice Abyss region. The model employs a multi-criteria decision analysis, integrated with hydrological modeling and a high-resolution random forest-based prediction algorithm, to downscale land surface temperature (LST) in order to obtain high-resolution 1 × 1 m spatial results. The primary contribution of this research lies in its capacity to assess not only the core objectives of groundwater protection but also its wider environmental impacts, including enhanced stormwater retention and the mitigation of land surface temperature increases. Key model predictors include land use and land cover data, and the framework is adaptable across diverse landscape types. In the case study area, water retention capacity demonstrated an increase of up to 30%, with an average rise in precipitation retention of 18.2 mm per microbasin. However, reductions in surface temperature were more modest, with a maximum decrease of 7.3%, corresponding to an average temperature drop of 1.5 °C. The model further identified pronounced seasonal and land-use-specific variations in surface temperature, particularly on agricultural land, where temperature fluctuations reached up to 2.6 °C between pre- and post-harvest periods. The findings of this study offer critical insights into how targeted land-use interventions can not only safeguard groundwater resources but also enhance landscape resilience to climate change. As such, this modeling approach provides an essential tool for the advancement of sustainable water resource management and climate-adaptive environmental planning.

Keywords: landscape planning; stormwater retention; land surface temperature; multicriteria analysis; Hranice Abyss

check for updates

Citation: Sedláček, J.; Vavrouchová, H.; Chytrý, K.; Ulrich, O.; Oppeltová, P.; Geršl, M.; Kohoutková, K.; Klepárník, R.; Kučera, P.; Vlček, V.; et al. Spatially Explicit Model for Assessing the Impacts of Groundwater Protection Measures in the Vicinity of the Hranice Abyss. *Land* **2024**, *13*, 1747. https://doi.org/10.3390/land13111747

Academic Editors: Alexei Konoplev and Afshin Ghahramani

Received: 30 August 2024
Revised: 20 September 2024
Accepted: 9 October 2024
Published: 24 October 2024

Copyright: © 2024 by the authors. Licensee MDPI, Basel, Switzerland. This article is an open access article distributed under the terms and conditions of the Creative Commons Attribution (CC BY) license (https://creativecommons.org/licenses/by/4.0/).

1. Introduction

Contemporary landscape planning faces unprecedented challenges in responding to global stimuli represented by climate change [1,2], the global economic situation, and at the same time in reflecting specific requirements of communities, stakeholders, and

natural and cultural features of a specific place or region [3]. The temperature change impacts are essentially manifested by a change in the precipitation regime, and temperature changes that impact through higher frequency of torrential rainfall events, floods, heat waves, or extreme meteorological phenomena. Besides property damage, the consequences of these climate change impacts also damage natural resources, e.g., by increased soil erosion, eutrophication of waters, biodiversity loss through the spread of non-native species, or natural retreat from original habitats. The challenges are examples of multisectoral solutions, the scope of which covers urban planning, water management, agriculture and forestry, stakeholders, and designer professions [4], considering different development scenarios [5].

Land-use change is a global issue that threatens biodiversity and the provision of ecosystem services to humans [6]. To mitigate the effects of land-use change, the concept of green infrastructure (GI) has been incorporated into spatial planning, aiming to recognize its benefits to human well-being [7,8]. The European Union's GI strategy [9] defines green infrastructure as "a strategically planned network of natural and semi-natural areas with other environmental features designed and managed to deliver a wide range of ecosystem services". These services range from biodiversity conservation to environmental, social, and economic benefits, with multifunctionality being an intrinsic characteristic of GI. Multifunctionality is a key concept because it enables both humans and the environment to use limited space more effectively [10]. This approach fosters dialogue with stakeholders regarding their preferences and the relevance of GI networks [11]. Therefore, selecting criteria that reflect local conditions and community preferences is essential for meaningful planning. The key problem areas in the presented case study were identified through a participatory process conducted between April 2022 and August 2022, involving 150 participants.

In the present landscape planning discourse, great attention is also paid to solutions incorporating natural processes in dealing with issues related to adaptation to climate change. So-called Nature based solution (NbS) in connection with green infrastructure (GI) represents a scientifically validated approach with environmental, economic, and socio-political benefits [12,13]. These are then manifested in a wide range of benefits, from climate adaptation benefits [14], hydrological benefits [15] or cultural benefits [16]. Current research considers the multifunctionality of GI [17] in five thematic groups: (1) planning methods for urban GI, (2) assessment approaches of urban GI, (3) ecosystem services and their benefits, (4) sustainability and climate adaptation, and (5) urban agriculture. The multifunctional nature of GI is an important aspect of planning that relates to the outcome of measures and their functionality; it could be the integral part thereof [10,17,18]. Support or use of GI elements will manifest on multiple levels (e.g., the transformation of cropland to grassland (meadows) modeled in the paper will improve the infiltration capacity of the area, support biodiversity, and improve the absorbing (buffering) capacity of the area). When designing specific NbS measures, it is appropriate to apply a participatory approach [19,20], which shall facilitate the process of implementation [21,22].

Scenario analysis (SA) is an important part of supporting spatial planning and GI planning [23]. SA does not mean predicting the future state, but possible alternatives arising from defined assumptions and relationships [5]. Scenarios can be designed to explore the possibilities of achieving specific outcomes (e.g., reducing the temperature in a district, increasing the recreational potential of an area, watershed resilience [24] or creating a contrasting scenario allowing a comparison of the spectrum of impacts of different policy measures [25,26] including assessing the effectiveness of investments in GI in the context of the ecosystem services provided [27]. Mahmoud [25] further defines the concept of anticipatory scenario, i.e., a scenario based on desired or, conversely, undesirable visions of the future that may be achievable or avoidable if the necessary actions are taken currently.

In the context of climate change, it is necessary to consider a number of unpredictable phenomena and extreme events. Planning must therefore respond to these uncertainties while providing clear evidence for decision-making; in this regard, Miller [28] presents a new approach, scenario-based decision analysis, which integrates commonly used tools

of scenario planning and structured decision-making. In this context, particular attention should be paid to karst areas [29,30].

The aim of the presented case study is to delineate ecological regionalization by focusing on three critical landscape ecological risks: groundwater vulnerability, water retention capacity, and the effects of land surface temperature. The findings will provide recommendations for the sustainable development of the Hranice Karst area, which is renowned for its mineral springs and spas. Since the 1970s, this region has seen a marked intensification of agricultural activities [31], resulting in increased pollution of both surface and groundwater. Furthermore, intensive agriculture has led to a reduction in green landscape areas, which are vital for enhancing water retention capacity and mitigating temperature increases. These risks are compounded by the effects of climate change [1,2].

The second objective of this study is to provide detailed, scenario-based insights into selected GI benefits, with a focus on restoring the ecosystem's provisioning capacity by restricting development and construction activities in vulnerable areas, while promoting more sustainable and ecologically responsible agricultural practices. The rationale behind the zoning process, which involves assessing the current situation and major risks, as well as subsequent scenario-based interventions, follows the six-step geodesign framework proposed by Steinitz [4]. The first three steps focus on analysis: (1) Representation, involving the collection of data to represent the territory; (2) Process understanding, which entails examining the processes occurring within the territory; and (3) Evaluation, aimed at identifying problem areas or bottlenecks. The final three steps pertain to intervention: (4) Implementing changes; (5) Evaluating the effects of these changes; and (6) Making informed decisions regarding future modifications. This study provides an illustrative example of how a spatial planning framework can be effectively applied to support policy decisions in alignment with the European Union Biodiversity Strategy for 2030 [32], the Green Deal [33], and the Nature Restoration Law [34].

The vulnerable karst regions examined in this study serve to illustrate the potential of an integrated approach in assessing complex landscape relationships within a knowledge-based decision-making framework. The crucial role of spatial planning in protecting karst areas and implementing land use changes to support ecosystem services is further emphasized by Xiong and Li [30]. Due to their unique properties, karst regions allow little time for pollutant filtration or sorption, making them particularly vulnerable to surface-loaded contamination [25]. However, the dynamic and complex hydrogeology of karst aquifers complicates efforts to accurately characterize their vulnerability [29].

2. Materials and Methods

The paper presents a method for assessing (in terms of problem analysis, see [4]) and evaluating the effects of land-use changes in a specific karst area where mineral waters susceptible to contamination are present. The assessment and evaluation method consists of two steps (Figure 1).

The first step is to assess the processes within the territory to identify the relatively problematic (hot spots) and relatively stable (cold spots) locations regarding groundwater vulnerability, land surface temperature, and stormwater retention. The selection criteria is based on a combination of evaluations by an expert group responsible for the case study (elaborated on in their respective Sections later), input from the involved municipalities, and a public opinion survey.

Public participation and the identification of residents' preferences are integral components of the geodesign framework [4] A pilot online survey of residents was conducted between April 2022 and August 2022 with 150 participants. One of the two parts of the survey focused on residents' attitudes toward threats that could affect their immediate environment, with a particular focus on threats related to climate change. The pilot survey revealed residents' concerns about the negative impacts of climate change. They are particularly concerned about drought and lack of drinking water, as well as more frequent storm rains and extreme temperatures in the summer months. The combination of these

three threats is a concern for more than half of the respondents (55%), while the other threats (soil erosion, landslides, impacts of excessive tourism, and landscape changes) are considered less important. Most respondents agree with the statement that the landscape will be negatively affected by the effects of climate change and prefer nature conservation and active landscape management.

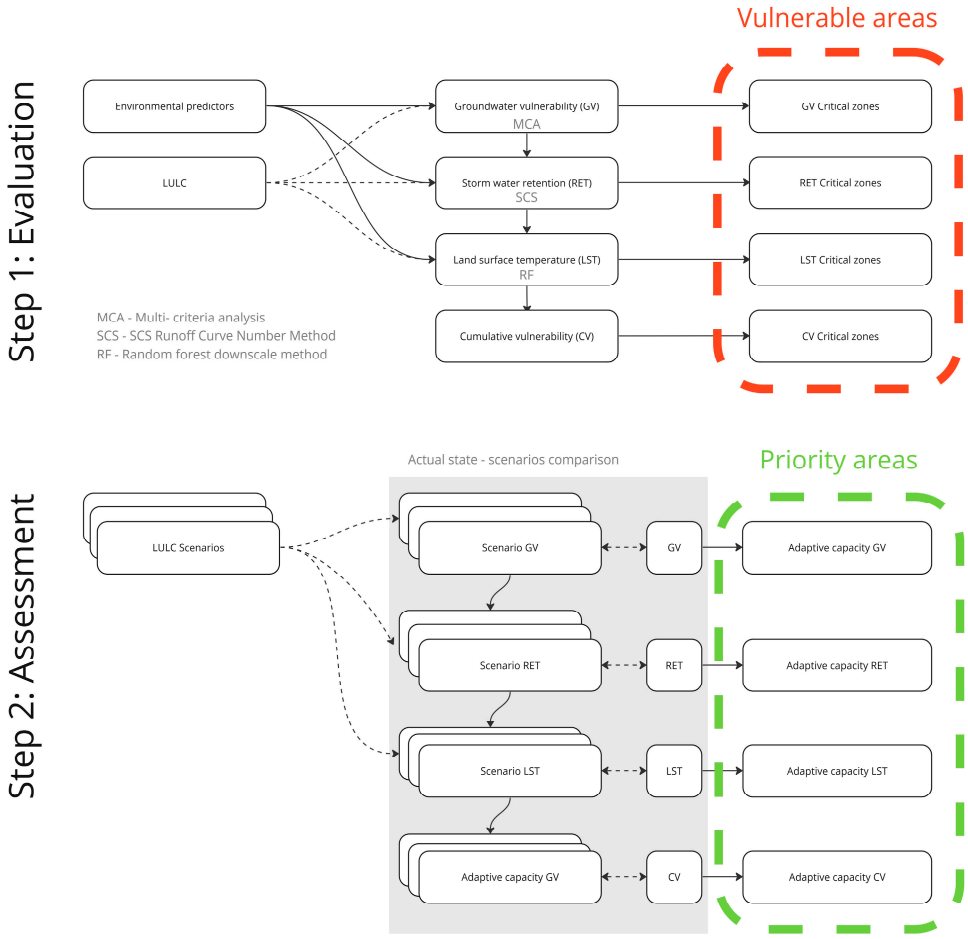


Figure 1. Research approach diagram.

The cumulative effect of all three criteria was compared using the so-called cumulative vulnerability method. The individual criteria were standardized to the values 0–1 to enable mutual combination. Groundwater vulnerability, land surface temperature, and surface runoff results were normalized to values from 0 to 1 to compare datasets. The normalization was then calculated using the following formula:

$$X'ij = \frac{Xij - Xmin}{Xmax - Xmin}$$

where X′ij represents the normalized value of the jth criterion in cell i, Xij is the raw model output of the jth criterion in cell i, and Xmin and Xmax, respectively, represent the minimum and maximum value of Xij. Normalization was calculated with the SAGA Raster Normalization Tool in the QGIS environment.

The normalized values were compared according to the formula:

$$\text{Vulnerability} = \frac{\text{Crit1} + \text{Crit2} + \text{Crit3}}{3}$$

where Crit1 represents Groundwater Vulnerability (Section 2.1), Crit2 stands for Stormwater Retention (Section 2.2) and Crit3 is Land Surface Temperature (Section 2.3). The result is

a raster representation with 1 × 1 m resolution. The raster layer was then converted to individual spatial units (microbasins, see Section 2.7) using the Mean tool in Zonal Statistic tool in QGIS version 3.28 [35].

The second step was to evaluate the future land use scenario. Each microbasin has a specific character due to its environmental factors and land use. In some microbasins, changes are therefore impossible, for example, in forest areas or flat areas where changes in land use increase the landscape's retention capacity. In this case, test scenarios based on so-called adaptive capacity were used to determine which areas would be most affected by the measures. Adaptive capacity represents the extent to which a change in land use can improve the given criterion [36]. The calculation is based on a difference between the existing value and the modeled scenario:

$$\mathrm{R}(\%\ \text{reduction}) = \left(1 - \frac{\mathrm{Crit1ac}}{\mathrm{Crit1sc}}\right) * 100$$

where Crit1ac represents the value of the criterion in the existing state, and Crit1sc represents the value of the criterion in the proposed scenario. The result is a 1 m GSD resolution map with R values representing the degree of reduction of the given problem. These values were then averaged again for the individual basins.

2.1. Groundwater Vulnerability Analysis

The Hranice Karst area is distinguished by its unique karst landscape, which is highly sensitive to contamination. Karst aquifers are particularly vulnerable due to their rapid water flow and limited filtration capacity, making them especially susceptible to pollutants from agricultural runoff, industrial activities, and other surface contaminants. The area under consideration in this case study is also part of the Protection Zones for Water Sources and Spa Areas, which are legally delineated around the most valuable recharge zones in the Czech Republic [37]. While numerous research activities have examined water quality, a comprehensive study that would inform land-use planning decisions to minimize contamination risks is lacking [38,39].

Foster [40] defines the concept of groundwater vulnerability as "natural characteristics, which influence, at variable levels, the sensitivity of multiple parts of an aquifer affected by an imposed contaminant load". The presented approach issues from the so-called intrinsic vulnerability, which focuses "solely on a theoretical-immutable pollutant particle's travel time affected by the hydrological, geological, and hydrogeological conditions; this evaluation considers neither the pollutant type nor the pollution scenario" [41,42], when unlike in specific vulnerability [41], vulnerability to specific pollutants is not covered. The selection of the parameters and the evaluation methods have also been adapted to this approach.

Due to the limited information available about the area, multi-criteria analysis (MCA) was used to determine the area's vulnerability based on nine criteria (Table 1). The multicriteria analysis is based on documented phenomena, which are divided into five categories (class elements) for each criterion, similar to the COP method [43]. Weights are assigned to individual criteria based on the order of expert evaluation within a research team. The most important criterion was given points (Bi = k), the second most important was given k − 1 point (bi = k − 1), and so on, until the last (least important) was given one point (bi = 1). The weight of the relevant criterion was calculated as follows:

$$\mathrm{Wi} = \mathrm{Bi} / \sum_{\mathrm{i}=1}^{\mathrm{k}} \mathrm{Bi}$$

where Wi is the resulting weight of the criterion and Bi is the point rating of the criterion.

Table 1. The input data for the multicriteria analysis.

Criterion	Class Element (4—Highest Risk, 0—Lowest Risk)	Weight
Hydrogeological aquifer	Cavernous karst-type aquifer: 4 Porous aquifer: 2 Fractured aquifer—2 (high transmissivity increases the class, low transmissivity lowers the class) Confining unit: 0	7/43 = 0.16
Hydrological soil groups	Type A: 4 Type B: 3 Type C: 2 Type D: 1	8/43 = 0.18
Geological substratum	Unconsolidated fluvial sediment: 4 Eluvium, stony-sandy: 3 Unconsolidated loess-clay sediment: 3 Unconsolidated calcareous clay sediment, breccia: 4 Deluvial sediment: 2 Unconsolidated sediment, loess clay: 1 Unconsolidated sediment, calcareous clay: 1	9/43 = 0.21
Land use/Land cover	Cropland: 4 Meadows: 2 Forestry: 0 Green Infrastructure: 1 Industry and Commerce: 4 Institutional: 3 Limestone quarry: 4 Mixed, Higher Density and Commerce: 3 Residential, Low density: 2 Spa: 2 Transport Infrastructure: 2 Water Infrastructure: 4	4/43 = 0.09
Documented karst phenomena (caves, abyss, sinkhole) orthogonal projection onto surface + distance in meters	25–0: 4 50–25: 3 75–50: 2 100–75: 1 Over 100: 0	6/43 = 0.14
Potential karst phenomena + distance in meters	25–0: 4 50–25: 3 75–50: 2 100–75: 1 Over 100: 0	5/43 = 0.12
Drains	Present and documented: 0 Absent: 3	1/43 = 0.02
Hydrological model	Division based on drainage, 5 classes (5-class quantile), places with the highest drainage have the highest value	3/43 = 0.07
Technical infrastructure in meters	Sewerage + 50 m distance	2/43 = 0.05

Individual criteria were converted to a raster with the same 1 m GSD resolution and using a raster calculator in QGIS software v. 3.28, the resulting value for the given area was calculated.

$$\mathrm{Vgw} = \frac{\mathrm{Crit1} * \mathrm{W1} + \mathrm{Crit2} * \mathrm{W2} + \mathrm{Crit3} * \mathrm{W3}}{\sum_{i=1}^{k} \mathrm{Wi}}$$

The resulting grid shows the risk to the area on a scale of 1 to 0 and at a resolution of 1 × 1 m. Value 1 represents the maximum vulnerability in the area of interest (AOI),

and value 0 means the minimum vulnerability of the area. To identify critical basins, the Zonal Statistic tool was used to calculate the average for each basin, dividing the values into five classes (see Section 2.7) and distinguishing them graphically using the same interval method.

2.2. Stormwater Retention

The ability of a landscape to retain stormwater is essential for effective water resource management, flood prevention, and the maintenance of the water cycle, particularly in regions characterized by intensive agriculture. In the Hranice Karst area, the expansion of agricultural activities has led to a reduction in green spaces, consequently diminishing the region's natural capacity for stormwater retention. The area is prone to erosion, and the two municipalities, Černotín and Hluzov, are particularly susceptible to flash floods. According to the Intergovernmental Panel on Climate Change [44] and the European Environment Agency [45], climate change is expected to exacerbate this situation. Zeder and Fischer [46] further highlight that the intensity of extreme precipitation has increased at nearly two-thirds of meteorological stations from 1901 to 2013.

To calculate stormwater retention, an effective precipitation calculation equation based on the SCS (Soil Conservation Service) Runoff Curve Number Method [47] was used. This is a calculation of the direct runoff from the basin, which relies on so-called effective precipitation and temporarily retained precipitation. Precipitation volume is converted to runoff volume based on the CN runoff curves based on the hydrological properties of the soils. The CN value depends on the combination of the hydrological soil group, the index of previous precipitation, and the land use type in the respective area. This method takes into account soil water retention, initial saturation, and land use of the area in question but is only suitable for modeling short scenarios as it does not take into account soil water saturation, which occurs gradually over the course of a rainfall event.

For the area, CN Urban Hydrology tables for Small Watersheds, known as TR-55 [48] and a method by Janeček [49] were used. This method classifies different land cover types and their hydrological status in detail. For surface assessment, a LiDAR classified point cloud was used to identify different vegetation types (see Section 2.6).

The retention capacity of the area is calculated from the difference between total precipitation and effective precipitation using the following equation:

$$R = P - \frac{(P - 0.2 * S)^2}{(P + 0.8 * S)}$$

$$S = \frac{1000}{CN}$$

where R stands for the maximum value of retention in inches converted to mm, S is the maximum retention at the beginning of the rainfall event, and P is precipitation in mm.

Surface slope is not taken into account in the original CN method, although slope has by no means negligible effects on water infiltration into the soil, i.e., on the resulting amount of effective precipitation. Currently, when detailed data is available to create digital terrain models, it is convenient and relatively easy to project the terrain slope onto the CN values. Therefore, these were projected onto the CN curves using the Sharply–Williams method [48]:

$$CNSW = \frac{1}{3}(CNw - CNm)(1 - 2e - 13.86\alpha) + CNm$$

$$CNw = \frac{100 * CNm}{43 + 0.57CNm}$$

where CNSW is the slope-adjusted CN by Sharply–Williams's method, and CNw is CN for wet soil moisture condition. The CNm represents CN for moderate soil moisture condition, and α is terrain slope m/m.

The total precipitation was assumed to be 2 h N100, which, according to the DES RAIN software (Version 1), is 86–15 mm. DES RAIN is a software for modeling precipitation in the Czech Republic [50]. Precipitation is torrential rain lasting 2 h that occurs once in 100 years, with data based on long-term measurements between 1901 and 1980. The initial loss was determined to be 20% of the maximum retention potential. The calculation diagram is included in Appendix A: Diagram of Containment Capacity Calculation Using SCS-CN Method Modified from Sharply–Williams Applied in This Study.

2.3. Land Surface Temperature Analysis

Surface temperature is a crucial indicator of a region's thermal dynamics, significantly impacting both human and ecological health. In the Hranice Karst area, intensive agriculture and land-use changes have resulted in a reduction of vegetative cover, which naturally regulates temperature through shading and evapotranspiration. The area falls within a region with a high probability of an increase in the frequency of heatwaves due to climate change [51].

The exchange of air masses between urban and rural areas is essential for mitigating the urban heat island effect, as demonstrated in various strategies [52], such as those implemented in the Neckar Valley [53] and the Danube-Iller region [54]. The terrain configuration in the case study area suggests the potential for creating so-called "heat sinks" that could cool urban areas during nighttime hours. By focusing on surface temperature, this study emphasizes the need for climate adaptation strategies that can reduce heat stress and improve the overall livability of the region.

For the area under study, five scans from the LANDSAT 8 satellite [55] with a cloud cover range <10% and a resolution of 30 × 30 m were selected, which captured the area from 29 May to 18 September 2023. Downscaling land surface temperatures (LST) from satellite images is essential for many fine-scale applications and there are various methods for its application [26]. For downscaling, the random forest model [56] was used, e.g., Hutengs and Vohland [57] which applied to LST. The downscaling method was used due to the complex topography of the land cover in individual microbasins, and to include small fragments of vegetation such as linear vegetation along property lines, individual trees, and scattered vegetation in parks that could be included in scenarios.

To relate the LST to LULC, which has a resolution of 1 × 1 m, it was necessary to downscale the LST to a resolution of 1 × 1 m using topographic predictors derived from a digital terrain model. Specifically, the Topographic Wetness Index, Slope Gradient, Topographic Prominence Index, and Radiation Index were used. To fit the model, a sample of 3000 areas selected through stratified random sampling (SRS) was used, taking into account the above-mentioned variable environment and land use (see Figure 2). For SRS, K-means clustering to 10 different clusters was applied and then 300 random points were selected for each cluster. The model was fitted separately for individual periods as a different relationship in the dependence between LST and LULC was expected. The interval, which covers a large part of the growing season, was chosen mainly due to the different temperatures (LST) in the agrocenoses with regard to the phenology of the respective crop. The same model was then used to predict the respective LST per individual LULC (Section 2.6). To compare temperature fluctuations, the original measurements from the satellite images were not used, but rather the downscaled model, i.e., the model predicted for current land use. One reason for this was the coarser spatial resolution of the original satellite data. The other reason was to ensure that the LST data sources used for comparison were subject to a comparable level of error.

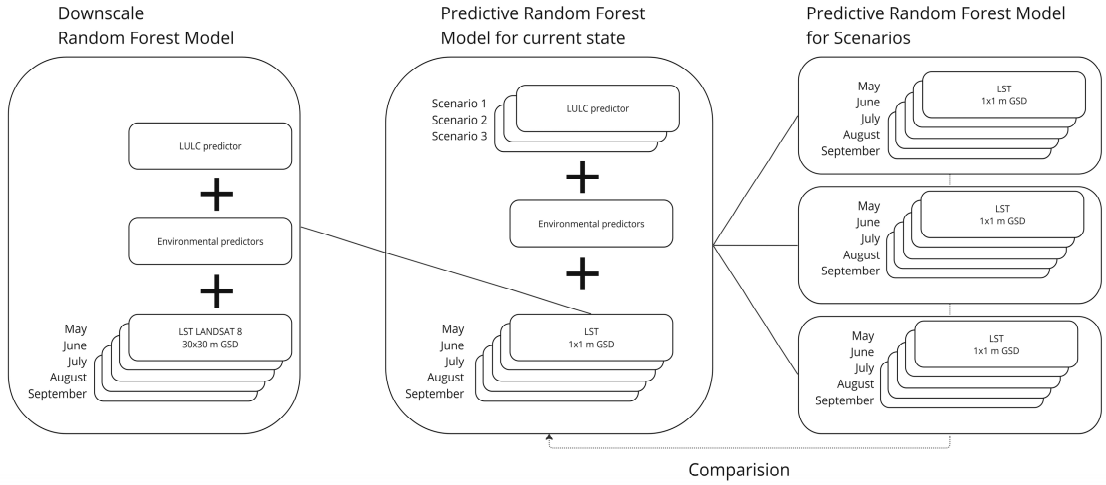


Figure 2. Diagram of the downscale and prediction of the Land Surface Temperature model.

2.4. Case Study Area

The Hranice Karst (Hranický kras) is the only hydrothermal (so-called hypogene) karst in the Czech Republic. It is located within a small protrusion (ca. 5 × 3 km) of Devonian and Paleozoic carbonate rocks in the eastern Czech Republic (49°31′ N, 17°45′17″ E ca. 100 km northeast of Brno (Figure 3)). Paleozoic carbonates are partially overlain by younger sediments belonging to the Neogene of the Subcarpathian region and consisting mainly of clays and sandstones [39]. The Quaternary cover consists of RSG-rendzic leptosols, arenosols, and regosols on the karst bedrock; RSG-luvisols or retisols and cambisols dominate on agricultural land (IUSS 2014/2015, https://openknowledge.fao.org/server/api/core/bitstreams/bcdecec7-f45f-4dc5-beb1-97022d29fab4/content, accessed on 1 October 2024).

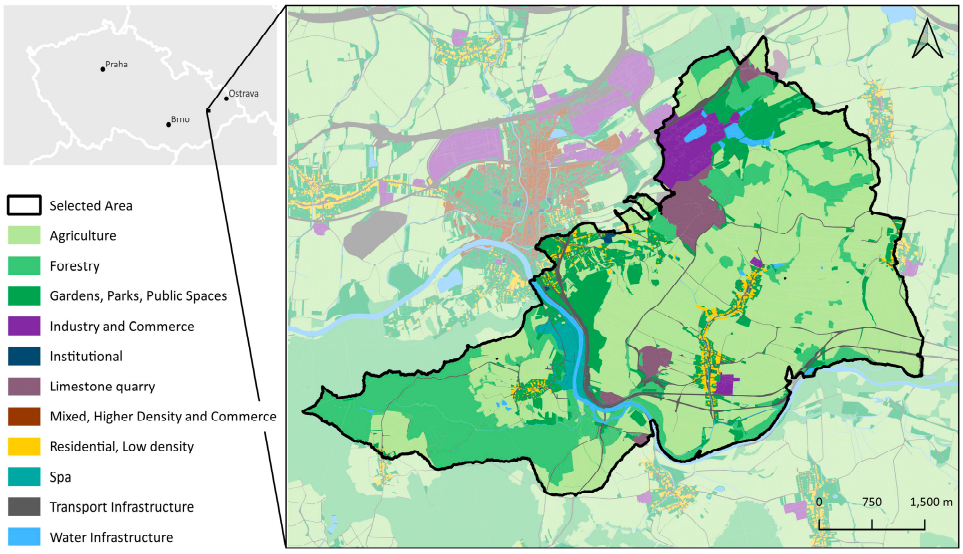


Figure 3. Wider context and location of the territory within the Czech Republic.

There are 30 limestone caves known in the karst area, the largest of which are the Zbrašov Aragonite Caves (ZAC) with their unique hydrothermal decoration and gas lakes with CO_2. The Hranice Abyss (HA), the deepest freshwater-flooded abyss in the world, is also located here. It is generally believed that the formation of the abyss and surrounding mineral springs in the karst area is associated with the influx of young CO_2 from deeper regions of the geosphere [58]. The abyss is filled with mineral water with high CO_2

content [39], and there are sources of hypogenic mineral water to a depth of 30 m, 40 m, and 60 m.

In the Zbrašov Aragonite Caves, there are also lakes with warm mineral water covered by a layer of gaseous CO_2. The seepage areas of the water from which the mineral waters are created have not yet been identified. However, it appears that the mineral waters arise from the mixing of older and younger waters and that some of the waters penetrate into the subsoil at slightly higher altitudes [39,59].

Bečva River and its tributaries drain the entire study area. In addition to surface waters, there are also drainage waters, and shallow and deep groundwaters (simple and warm mineral waters). Conclusions of the study by Sracek [39] show that the origin of karst water in the karst aquifer in the Hranice karst is meteoric in nature and there is a recharge area in the highlands about 200 m above the Bečva River valley. This assumption is also documented and substantiated by the vulnerability analysis performed.

2.5. Data Sources and Processing

Data used for the analysis included remote sensing, national geospatial databases, and field surveys—all data sources are listed in Table 2. Spatial analyses were performed in the ArcGIS Pro 3.0.2 [60] and QGIS 3.26. [35], satellite images were processed in SNAP (ESA), and statistical calculations were modeled in R environment in R Studio version 2022.12.02 [61]. Hydrological analyses were processed in QGIS, and precipitation estimation was based on DES-RAIN software [50]. A classified LIDAR point cloud with 50 points per square meter was used for the model area. Based on LIDAR data, hydrologically correct digital terrain, a digital surface model, and a canopy height model with relative heights of vegetation cover were created using the ANUDEM method [62]. Vector data were converted to a raster format with a resolution of 1 × 1 m.

Table 2. List of input datasets. (**a**) Input datasets; (**b**) Derived datasets.

(**a**)

Dataset	**Source**	**Data Type**	**Cartographic Accuracy/Resolution (m)/Point Density**
Cadastral maps	State Administration of Land Surveying and Cadastre	Vector polygons	1:1000
LPIS (Land Parcel Identification System)	Ministry of Agriculture of the Czech Republic	Vector polygons	1:5000
Zoning plans	Hranice na Moravě municipality	Vector polygons	1:5000
LIDAR	Primis. S.r.o.	Point cloud (LAS 1.4 [63]) Point cloud	50 points/square meter
Land surface temperature	USGS (Landsat-8)	Raster layer	30 × 30 m
Geological, Hydrogeological map	Czech Geological Survey	Vector polygons	1:50,000
Soil map	Research Institute for Soil and Water Conservation	Vector polygons	1:25,000
Karst objects[1]	Nature Conservation Agency of the Czech Republic [64]	Vector points	1:2000
Precipitation data	Czech Hydrometeorological Institute	Vector points, tabular data	1:2000
Potential karst object[2]	Authors survey	Vector polygons	1: 500
Sociological survey	Authors survey	Vector polygons, tabular data	

Table 2. *Cont.*

(**b**)			
Optimized Land use Land cover typology	Author classification	Raster dataset	1 × 1
Drainage	Research Institute for Soil and Water Conservation and UAV research	Vector polygons	1:500
Digital terrain model[3]	Authors' calculated dataset	Raster dataset	1 × 1
Digital surface model[4]	Authors' calculated dataset	Raster dataset	1 × 1
Canopy height model	Authors' calculated dataset	Raster dataset	1 × 1
Microbasins	Authors' calculated dataset	Vector Polygons	
Land surface temperature prediction raster dataset	Authors' calculated dataset	Raster dataset	
Rainfall retention raster dataset	Authors' calculated dataset		

2.6. Streamlined LULC Classification

The most detailed land use database in the Czech Republic is the cadastral map, which is evaluated to a cartographic accuracy of 1:1000 and updated weekly [65]. The disadvantage of this map source is that it records the legal status of the properties, but not their actual condition, and it lacks information about the current land cover, which has a significant impact on all three selected criteria [47,66,67]. For this reason, a special land use/land cover classification was carried out; it comes from the cadastral map, distinguishing between some functional areas and adding information about the vegetation (see Appendix B: Cadastral–Streamlined LULC converter). For this purpose, a point cloud from LiDAR aerial scans was used; it was classified according to the LAS 1.4 standard [63]. From the point cloud, a canopy height model was created based on the classified vegetation categories (Low vegetation, Medium vegetation, and High vegetation) at a resolution of 1 × 1 m. This was then divided by the height of the vegetation into "low vegetation" (1 ≤ height < 3 m) and "canopy cover" (height > 3 m). Vegetation with a height of <1 m was left out. The selected land use categories were seamlessly updated with vegetation information at a 1 × 1 m pixel level across the entire area (Figure 4).

2.7. Scale Consideration

The accuracy of layers in Geographic Information Systems (GIS) is usually determined by the layer with the highest available precision or by the layer serving as the reference. Land use is a parameter involved in each criterion, predicting groundwater vulnerability (see Table 1), stormwater retention (see Appendix A), and LST (see Figure 2). As one of the few observable parameters that can be quantified and defined on the surface, we considered it as the reference. In our methodology, we faced the challenge of whether to upscale the high-resolution land use data to match the lower resolution (30 × 30 m) LST and other layers. Following the aforementioned principle, where the layer with the highest resolution and accuracy serves as the reference, we opted to downscale all other elements to 1 × 1 m resolution. Another relevant reason for selecting LULC (Land Use/Land Cover) as a predictor and maintaining its high resolution is that it is the only parameter we can influence.

This approach makes it possible to carry out calculations for each cell individually, thus obtaining analysis results and impact predictions with high resolution. With regard to landscape management, it is advisable to find a unit that divides the area into larger segments. When selecting units, the following levels were taken into account: individual plots, parts of agricultural land blocks according to the Land Parcel Identification System (LPIS), areas with different types of land use according to the spatial plan, microbasins, and cadastral areas. For the final comparison, we chose the "microbasin" unit because microbasins are areas of approximately equal size that correspond to the natural distribu-

tion of the landscape and are suitable for management measures that improve drainage conditions in the area.

The entire area was divided into 98 microbasins using the Basin Tool (QGIS) based on the digital terrain model created by plotting the lines of water courses, adding solid objects (buildings), and removing drainless depressions (Table 3).

Table 3. Characteristics of the microbasin layer.

N	Area [ha] Min. Value	Area [ha] Max	Area [ha] Mean	Area [ha] Median	Area [ha] Standard Deviation	Area Coefficient of Variation
98	3.854	61.11	24.80	22.94	11.96	0.48

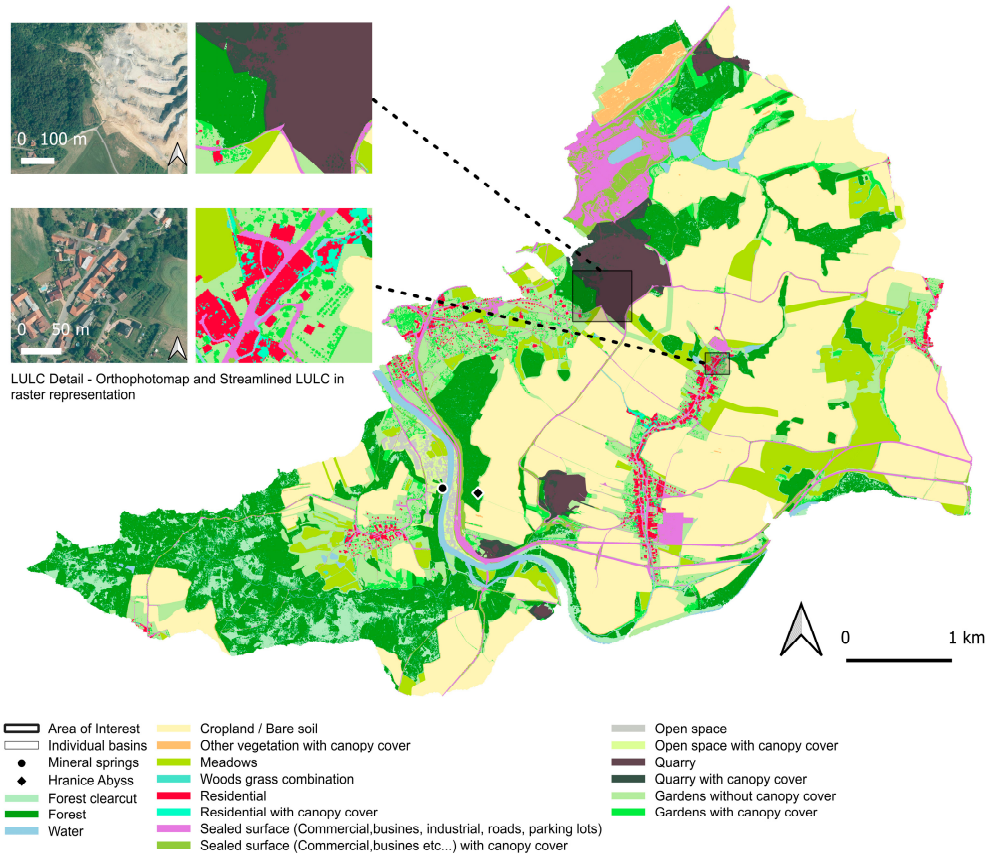


Figure 4. LULC updated with Canopy Height Model.

3. Results

The results are divided into two parts—the assessment of the territory in Sections 3.1–3.4 and the effects of the scenarios and their impact in Section 3.6. The purpose of this approach is to target measures to those parts of the territory where their impact is greatest in the observed parameters.

In the first part, the results of the analysis are presented. The assessment of the territory and the definition of problem areas are based on three selected parameters: groundwater vulnerability, rainwater retention, and surface temperature. Each of the parameters is evaluated separately and divided into five zones: 1 to 5, where Zone 5 represents a problem area with respect to the given parameter, and Zone 1 represents a problem-free area. The same approach was applied in assessing a combination of parameters—cumulative vulnerability—to define areas where a cumulative effect of the above parameters occurs. The values of the individual parameters are normally distributed; the equal interval classification method was used for the representation of the data.

In addition, two critical zones have been defined: a higher A and a lower B zone, which define problem areas mainly within Zone 1 and Zone 2 (in the case of rainfall retention also in Zone 3) and in locations adjacent to built-up areas. The critical areas represent the parts of the territory where measures to contain the phenomenon in question must be prioritized.

In the second part of the results, three different scenarios are applied; these scenarios are based on a land use change (LULC) from minimal to contrasting, where the impact of the measure is verified. The term "adaptive capacity" is used for the effect of the measure—the rate of improvement of the given parameter after the implementation of the respective measure—which is determined as a percentage change between the current and the target state.

3.1. Groundwater Vulnerability Areas

The vulnerable areas (Figure 5 left) overlap with the Maleník geomorphological unit (the Maleník fault block) in an area north of the Bečva River (4), around the municipality of Teplice nad Bečvou (6), and further down in the Bečva floodplain (2) and the Bečva Valley (1). Areas most at risk are concentrated around the Hranice abyss and on the slopes to the Bečva valley and east of the municipalities of Černotín and Hluzov (3). Apart from the sloping hillsides of the Bečva Valley, these basins are predominantly used as agricultural land. The areas of highest vulnerability were identified at the microbasin scale (critical zones 4 and 5, Figure 5 right). Measures to protect groundwater and mineral waters should be aimed primarily at this part of the territory.

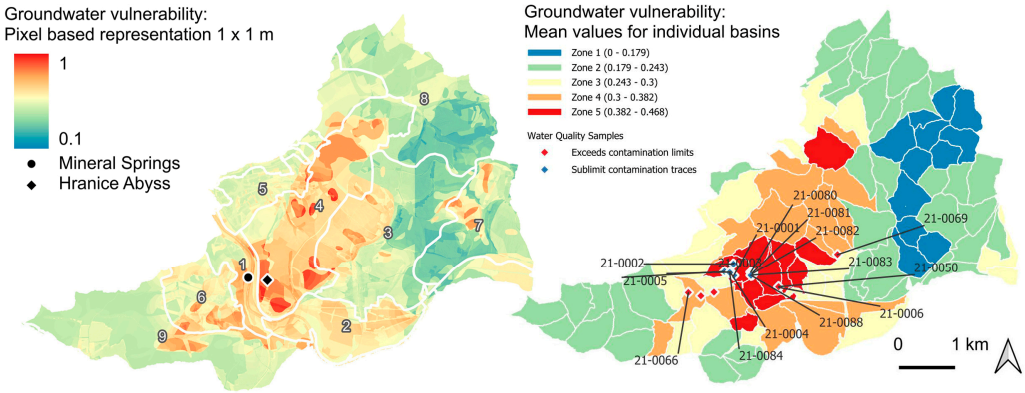


Figure 5. Groundwater vulnerability zoning. The result of the spatial multi-criteria analysis and its conversion to the individual catchment areas overlayed with samples.

The least vulnerable areas are in the southern part of the Maleník fault block (9) and in the eastern part of the territory outside the karst aquifer (7, 8).

To evaluate the zoning results, they were compared to water quality samples collected during the years 2021–2023 [38]. The water quality analysis revealed concentrations in groundwater that significantly exceed the values set by legal regulations, as well as sub-threshold values that indicate the vulnerability of the area. Figure 5 shows the overlay of the sample locations and vulnerability zoning; the table commenting on the samples is included in Appendix C.

3.2. Stormwater Retention Capacity

The total precipitation was considered as 2h N100, i.e., H. as precipitation with a frequency of once in 100 years, which according to DES RAIN software is 86–15 mm. The initial loss was determined to be 20% of the maximum potential retention [47]. The retention capacity for water bodies was determined to be 0 mm. The resulting map shows the retention capacity for AOI on a generalized basis per cell of the grid, with the highest value being 86.15 mm and the lowest value being 0 mm (Figure 6, left). With regard to hydrological retention measures that can be carried out within the microbasins, the retention capacity value is calculated as an average for the individual microbasins (Figure 6, right).

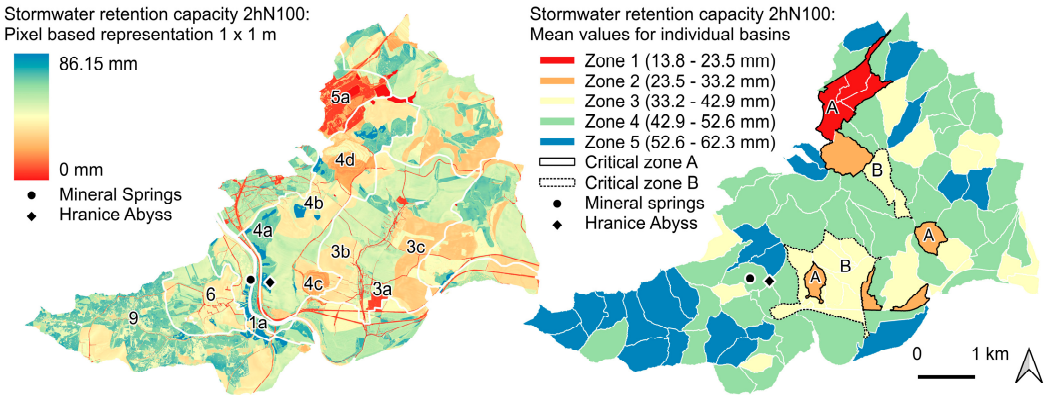


Figure 6. Retention capacity of the territory. The image on the left shows a grid with 1 m GSD resolution. The image on the right shows the retention capacity values recalculated as an average for each basin.

The forest stands in the Hůrka National Nature Reserve (4a), within the Malá and Velká Kobylanka nature reserves (4b), and on the southern slopes of the Bečva Valley (1a), and exhibits the highest stormwater capacity. This high retention potential is primarily due to the dense forest cover and the presence of soils classified under Hydrological Group A, which are known for their high infiltration rates and low runoff potential. The southern part of the Maleník fault block, characterized by a significant proportion of forested land, further demonstrates a notable retention potential, contributing to the area's resilience against stormwater surges.

In contrast, the industrial zones adjacent to the Hranice cement factory (5a) and the industrial facilities in the southern part of Černotín municipality (4c) exhibit the lowest retention capacity. This is due to the predominance of impervious surfaces, which inhibit infiltration and increase surface runoff, thereby reducing the overall retention potential. Additionally, the cultivated areas on the slopes east (3b) and west (3c) of Černotín also demonstrate low retention capacity, a result of the combined effects of steep slopes, soil types with low infiltration capacity (Groups C and D), and land use dominated by cropland, which further exacerbates surface runoff and reduces groundwater recharge.

Critical zones with heightened groundwater vulnerability were identified at the boundaries of several microbasins. Critical Zone A, encompassing the industrial areas near the Černotín cement factory, including the Hranice quarry, is particularly susceptible due to the extensive modification of natural landscapes and the presence of impermeable surfaces. This zone also includes microbasin areas 3c and 3a, where the interplay of industrial activities and the geomorphology of the area contribute to the elevated risk of groundwater contamination and reduced retention capacity.

Similarly, the second critical zone, located east of Černotín (B) and east of Hluzov (B), was identified as particularly vulnerable due to its proximity to residential areas. These microbasins are at risk primarily because of their position downstream from cultivated lands with low retention capacity, where increased surface runoff can lead to localized flooding and potential contamination of groundwater resources. The detailed zoning of these areas highlights the need for targeted stormwater management strategies to mitigate risks associated with both low retention capacity and groundwater vulnerability.

3.3. Land Surface Temperature

The results of this study are derived from the analysis of LANDSAT satellite imagery and predictions generated by a random forest model (detailed in Section 2.3). The model's predictions for May exhibited significant discrepancies compared to the observed conditions (refer to Appendix D: Difference between prediction model and measured condition (°C)), leading to their exclusion from further analyses.

The analysis of the satellite images (Figure 7) reveals distinct patterns of surface temperature anomalies across the study area. Specifically, areas consistently exhibiting higher temperatures than their surroundings were identified as heat islands. These heat islands are predominantly located in built-up residential areas and active quarries. The primary sources of these temperature anomalies include the following:

- Industrial Areas (A1): The industrial zones, particularly the Černotín industrial facilities, are characterized by extensive impervious surfaces, which absorb and retain heat, leading to elevated surface temperatures.
- Quarries (A2 and A4): The Hranice and Černotín quarries also serve as significant heat islands. The lack of vegetation and the presence of exposed rock surfaces in these areas contribute to higher thermal retention and surface temperatures.
- Residential Areas (A3, A5, A6, and A7): The residential areas zones of Teplice nad Bečvou, Černotín, Hluzov, and Hranice exhibit elevated temperatures due to dense urbanization, limited vegetation, and the prevalence of heat-retaining materials like concrete and asphalt.

In contrast, areas that consistently display cooler temperatures relative to their surroundings include the following:

- Hůrka National Reserve (B1): The dense forest cover in this protected area provides a cooling effect, reducing surface temperatures significantly.
- Forests East and South of Teplice (B2 and B3): These forested regions also maintain lower temperatures, attributed to the shading effects of trees and the cooling influence of transpiration.

Areas with significant intraseasonal temperature fluctuations were identified in the following:

- Croplands East and West of Černotín (C1 and C3): These agricultural lands show temperature variability due to changes in vegetation cover throughout the growing season, as crops are planted, mature, and harvested.
- Croplands within the Floodplain (C2): This area also experiences considerable temperature variability, influenced by the dynamic hydrological conditions that affect soil moisture and vegetation health.

To further explain these temperature patterns, Normalized Difference Vegetation Index (NDVI) images from the same dates were analyzed. The NDVI, which measures the density and health of vegetation, provides insights into how vegetation cover influences temperature patterns. For instance, areas with higher NDVI values, indicating denser vegetation, tend to exhibit lower temperatures due to the cooling effects of evapotranspiration and shading (see Figure 7: Intraseasonal LST variability in comparison with the Normalized Difference Vegetation Index).

The random forest model downscales temperatures based on land use and land cover (LULC), allowing for more detailed temperature predictions at finer spatial scales. The model consistently predicts a narrower range of temperature values compared to measured conditions (Appendix E: Comparison of the prediction model and the measured state for the 22 June 2023 sample). The highest surface temperatures were observed in quarries, sealed areas, and densely built-up residential zones. In contrast, the lowest temperatures were recorded in forests, forest clearcuts, and bodies of water, where vegetation and moisture play a critical role in moderating temperatures.

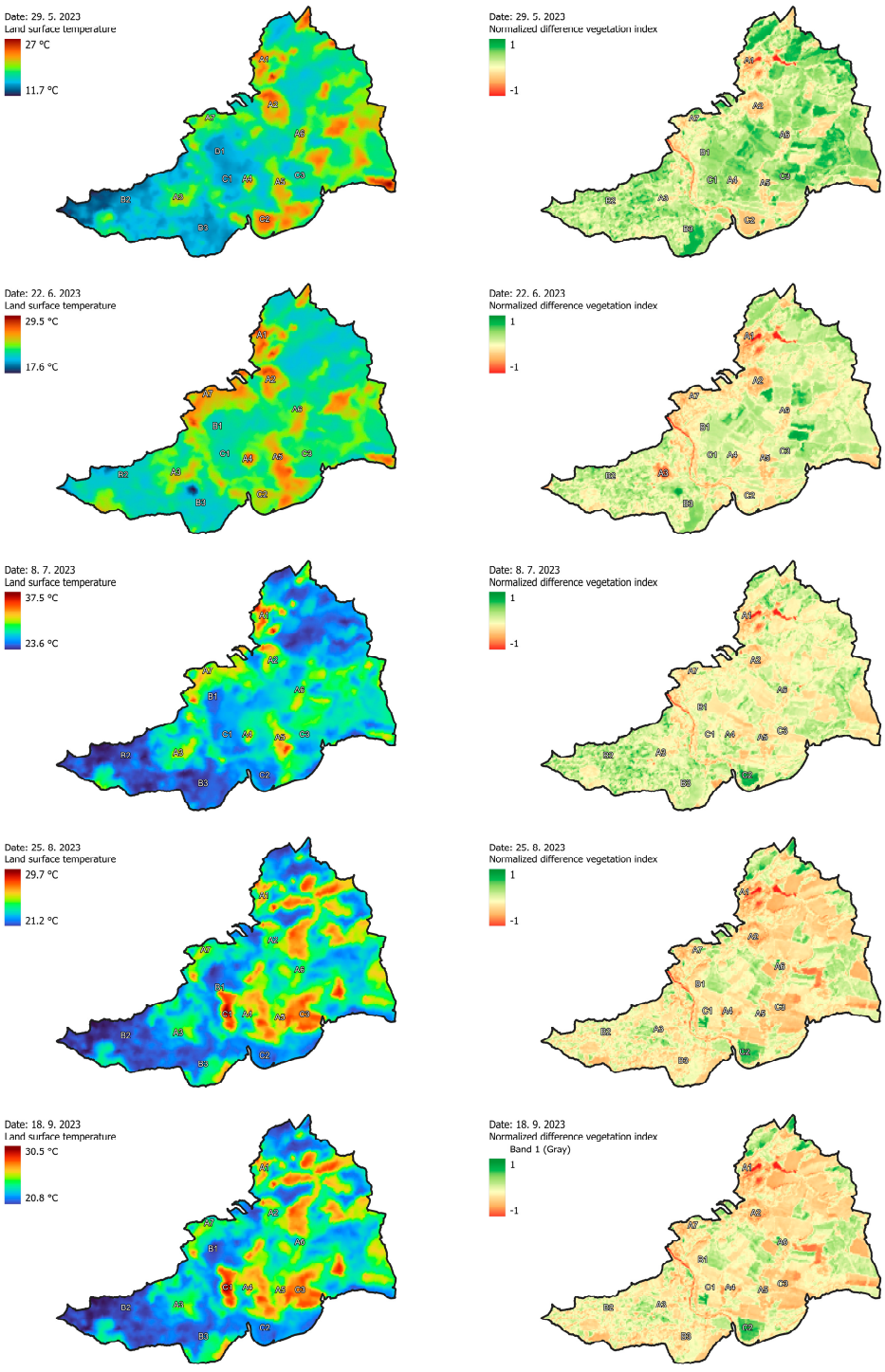


Figure 7. Intraseasonal LST variability in comparison with the Normalized Difference Vegetation Index.

For spatial representation at the microbasin scale, the average temperature from the entire measurement set (comprising five measurements covering the growing season from May to September) was used. The highest temperature categories were consistently found in the sealed areas and quarries, specifically in locations such as the Černotín quarry (A1), the Hranice quarry (A2), and the Černotín industrial facilities (A3) (Figure 8). Critical Zone B was determined within the heat islands of the municipalities, including the areas around Černotín (B1) and its adjacent landscape, Teplice nad Bečvou (B2), and parts of Hranice (B3).

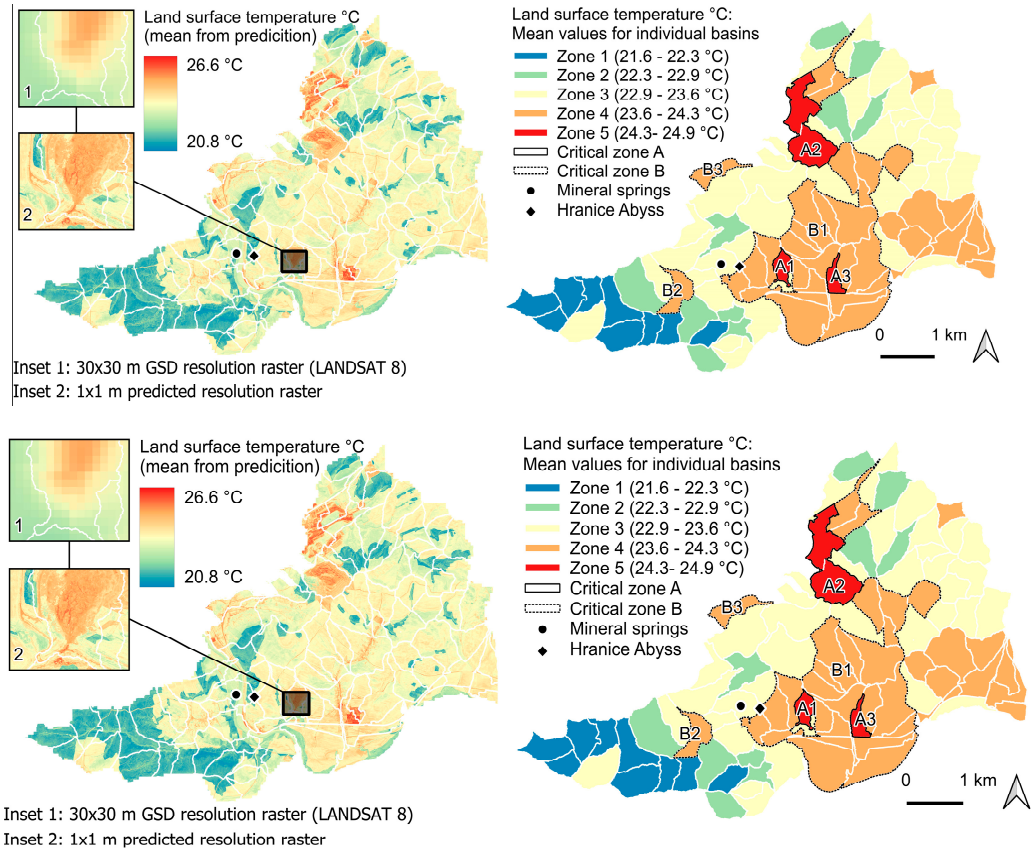


Figure 8. Result of land surface temperature prediction model and its mean for individual basins.

3.4. Cumulative Vulnerability

A cumulative effect of selected criteria was examined. To obtain comprehensive results, the relative impact of various factors was assessed. Three combinations of weights were considered: equal weights, increased weight for groundwater vulnerability, and increased weight for both groundwater vulnerability and stormwater retention capacity (see Table 4, Figure 9).

Table 4. Comparison of weights used for the cumulative vulnerability.

	Weights		
Weights Combinations	**Groundwater Vulnerability**	**Stormwater Retention Capacity**	**Land Surface Temperature**
Equal Weights	0.33	0.33	0.33
Increased Groundwater Vulnerability	0.5	0.25	0.25
Increased Stormwater Retention Capacity	0.4	0.4	0.2

To be able to compare the values in all three criteria, the data were normalized to the values 0–1. In the case of cumulative vulnerability, the values are relative and serve to distinguish the more vulnerable areas from the relatively resilient ones (Figure 9).

The comparison of the weights assigned to individual criteria illustrates their impact on the resulting zoning. This comparison was conducted based on the number of occurrences in critical zones (4–5) for all weight scenarios (Equal weights, Increasing the weight of groundwater vulnerability, Increasing the weight of stormwater retention), where presence in a critical zone counts as one point. The comparison distinguished areas that consistently appear in critical zones across all scenarios from those that show heightened sensitivity in only one or two instances (Figure 9). The figure further indicates which weight scenarios resulted in specific subcatchments being classified within the critical zone.

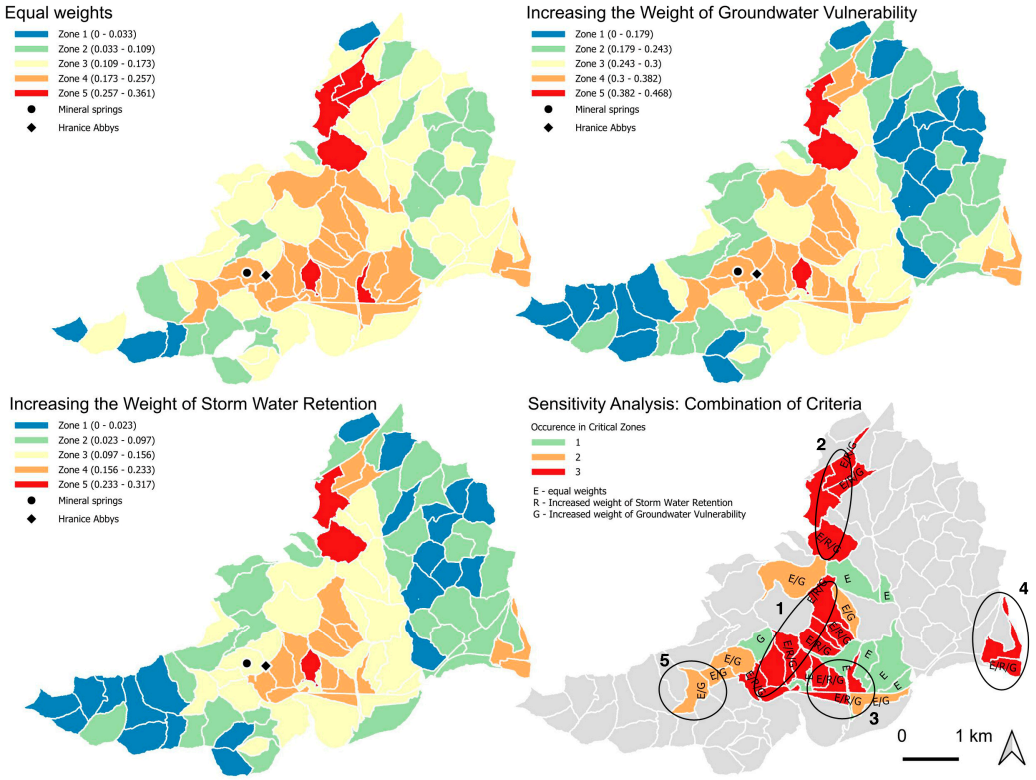


Figure 9. Comparison of different weights on selected criteria. The figure on the bottom right shows the frequency of microbasins in zones 4 and 5, representing vulnerable areas.

The most vulnerable areas were identified east of Černotín (1). These regions are intensively used for agriculture on karstic bedrock with low retention capacity. Another group of vulnerable areas includes quarries and adjacent industrial zones, notably around the Hranice quarry (2) and south of Černotín (3, 4). These areas, also situated on karstic bedrock, exhibit low retention capacity for stormwater and simultaneously act as heat islands. Areas characterized by increased vulnerability with respect to groundwater are located in the Teplice nad Bečvou region (5) and its surrounding outskirts, in catchments that are either built-up or predominantly covered by gardens and permanent grasslands.

3.5. Scenarios

Three hypothetical scenarios were formulated for the studied area: contrasting (scenario B), realistic (scenario C), and extensive (scenario D) (Figure 10). The scenarios focus on LULC changes in the undeveloped area. The aim is to use arable land less intensively, by partially converting it into grassland. This measure has been applied in karst areas and its effects have been confirmed [66,68,69]. The purpose of the "contrast scenario" is to determine the impact of the most extensive changes based on the conversion of cropland to grassland, the conversion of impervious areas to grassland (permanent grassland), the conversion of grassland and cropland to forest, etc. The "realistic" scenario 2 assumes the greening of cropland in the immediate vicinity of the Hranice abyss and the most vulnerable areas in the western part of the municipality of Černotín.

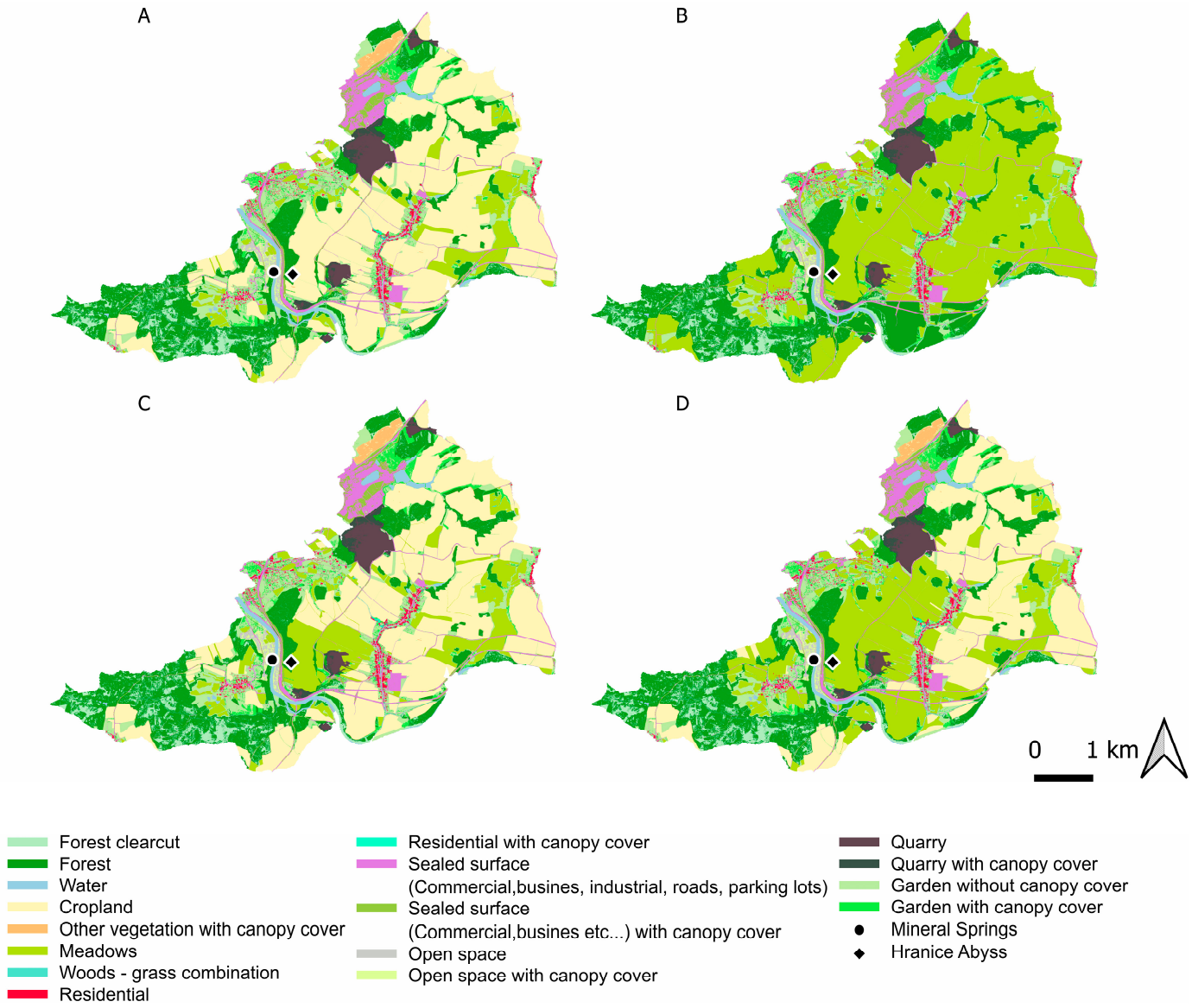


Figure 10. Overview of the current state of the LULC (**A**) and the scenarios: contrasting (**B**), realistic (**C**), and extensive scenario (**D**).

3.6. Adaptive Capacity

The effect of the individual scenarios was modeled as the ability to reduce a negative impact due to land use changes based on a calculation using the formula described in Section 2. This ability was expressed as a percentage change from baseline for each criterion individually and as an overall cumulative improvement. With the help of a spatial database, it is possible to select individual catchment areas, determine the values of the reduction potential according to individual criteria, and thus design a well-founded change proposal for the respective area.

The differences in impacts are significant (Figure 11). The changes in LULC have the greatest impact on increasing hydrological capacity in some catchments by 35% compared to the original state. If groundwater is at risk, the improvement occurs by smaller percentage points; the same applies to the reduction of land surface temperature (max. 8%) per individual catchment area. All data are averages per entire microbasin. As for temperature, the low adaptive capacity is determined by an average over the entire growing season. There are significant differences between cropland and grassland (according to the model, crops cool the surface more effectively than permanent grassland until early July).

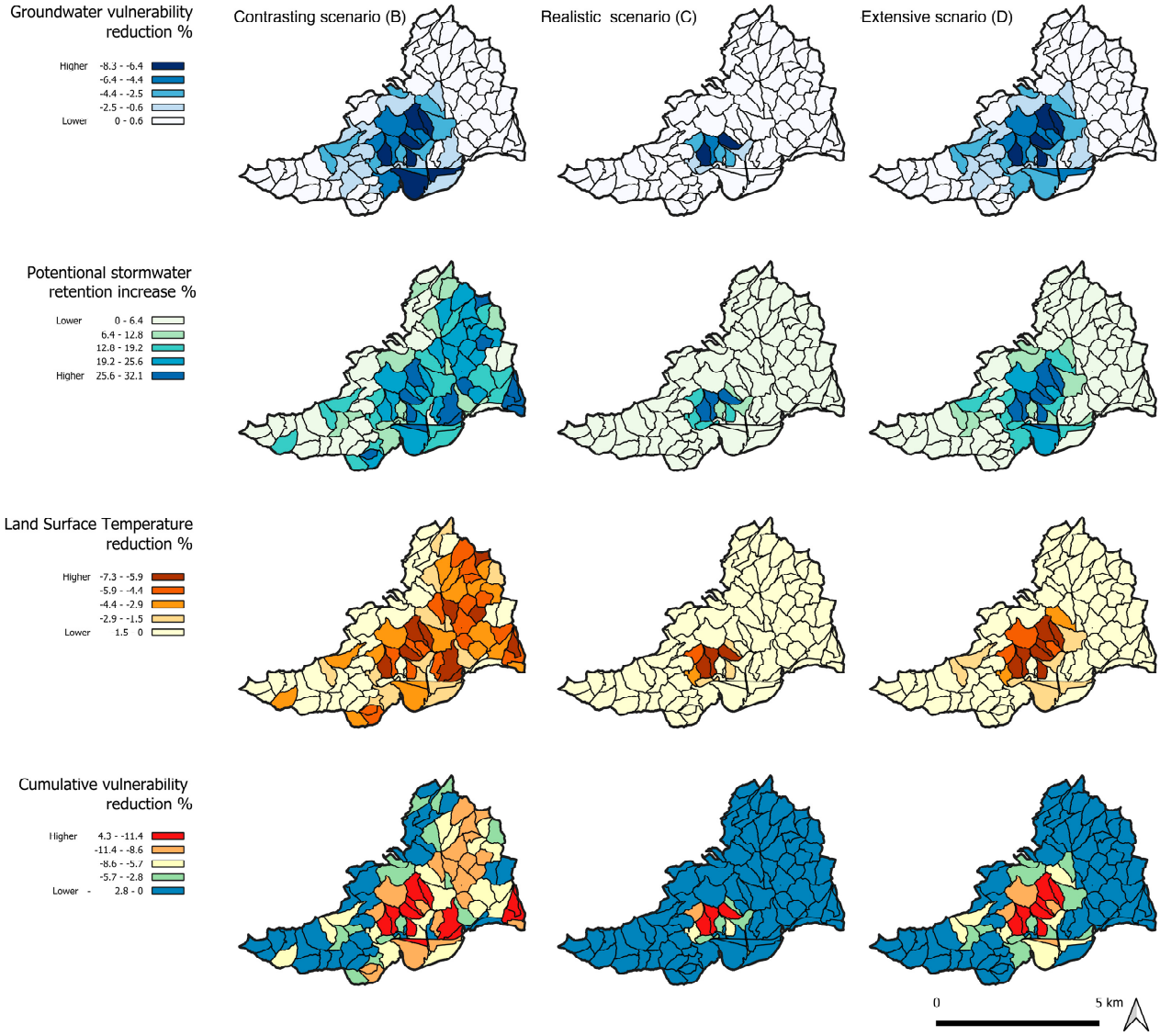


Figure 11. The effect of the individual scenarios was modeled as the ability to reduce a negative impact due to land use changes.

The overall rating combines all parameters in the Adaptive Capacity map. This combination enables a more precise focus on the areas where the measures have the greatest impact. From the individual scenarios, we selected and evaluated Zone 1 of the Adaptive Capacity Map, i.e., the area in which the measures have the greatest impact (Figure 12).

Main findings:

- The measures, which are primarily aimed at protecting groundwater, also affect other parameters—surface temperature and retention capacity—with an improvement of up to 30% in retention capacity, while there is only a reduction in surface temperature by 7.3%. Based on the hydrological model and the tailored prediction model, we are able to quantify the changes in these parameters.
- There is significant intraseasonal variation in surface temperature depending on the presence of crops.

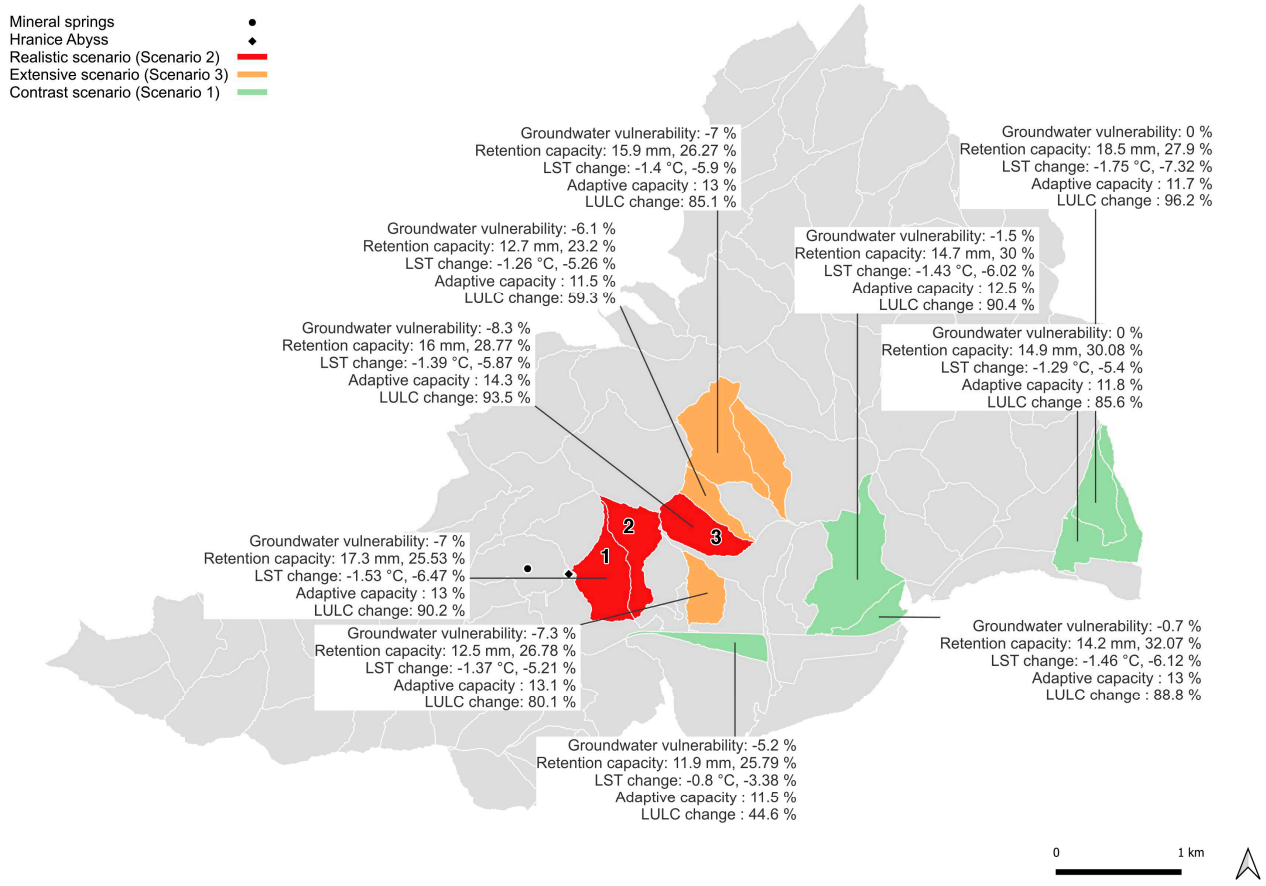


Figure 12. Evaluation of the impact of the scenarios on the observed criteria.

4. Discussion

Spatial planning and ecological science can both foster synergies and trade-offs [17]. Despite abundant literature referencing the multifunctionality of NbS and GI, there is a knowledge gap in the quantification of measures [17] and subsequent targeted focus on priority areas. Targeting of priority areas to mitigate the impact of heat was applied, e.g., by Madueira and Andresen [70] in Porto; combination of PM2.5, surface temperature, and stormwater retention [36] was used in Delft; Meerow and Newell [71] combined all the above phenomena with the accessibility of public parks, social vulnerability, and landscape connectivity in Detroit.

In this study, the approaches are transferred to a rural environment. The general view is based on the premise that rural areas also need to adapt to climate change [72], as 25% of the population in the Czech Republic lives in rural regions [73]. This need is all the more urgent as there is no structured and quantified approach to measuring the effects of GI [74] as inhabitants perceive it as critical Šilhánková et al. [75].

The study presents a method for assessing the benefits of measures to reduce a current problem—groundwater protection—with a broader problem of stormwater retention in preparation for climate change. Although areas to target on a relative scale were prioritized (Zones 1–5), it was possible to estimate surface temperature change in degrees and stormwater retention in mm for individual basins using data to quantify from remote sensing.

The study had to deal with the following knowledge gaps that still remain open:

- The model's resolution may not capture the fine-scale variations within microbasins and may miss small but significant areas that need protection or could benefit from targeted interventions.

- While the model suggests strategic changes, the actual implementation of these interventions may face practical, economic, or political challenges. The willingness and ability of local stakeholders to implement recommended actions may vary.
- The model focuses primarily on groundwater protection and the associated environmental parameters. The inclusion of other relevant factors such as socio-economic impacts and biodiversity considerations may be limited.
- The study does not use the specific COP, COPK method [44] for groundwater vulnerability studies or the DRASTIC method but instead uses an individual multi-criteria analysis commonly used in landscape planning.
- The intraseasonal changes in vegetation and their impact on surface temperature and retention capacity of the territory.

4.1. Intraseasonal Variability

Both the LST and hydrological prediction models are significantly influenced by the presence and type of crops grown. Depending on the vegetation phase, temperatures in agricultural cenoses change significantly (Figure 7). In the pre-harvest period, cropland has lower average temperatures than meadows, while in the post-harvest period, the opposite is true. This change reaches up to 2.6 °C (see Figure 13 and Table 5 below).

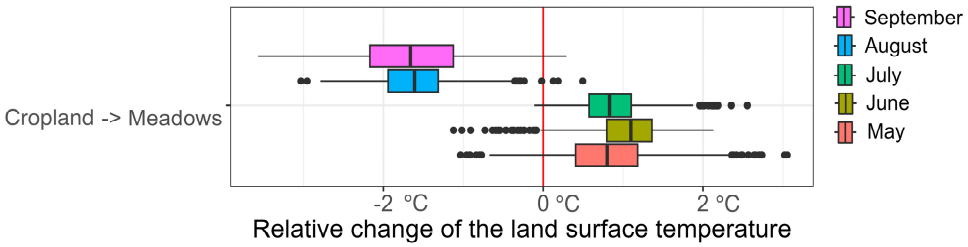


Figure 13. Temperature difference after conversion from Cropland to Meadows during the vegetation season.

Table 5. Cropland to meadow mean temperature change (°C).

	May	June	July	August	September
Cropland to Meadow	0.81	1.02	0.87	−1.60	−1.64

The presence of crops also significantly influences drainage conditions; when present, they increase retention capacity. The adaptation capacity was therefore determined based on the values at which the field retention capacity is lowest—when no crops are growing in the field. In the hydrological model, the bare soil parameter was determined at August temperatures, when the change from cropland to meadow indicated the highest change in LST. This assumption arises from the precautionary principle [76] that the highest risk is taken into account.

4.2. Spatial Granularity of Data

This study works with raster data that is evaluated on the basis of microbasins. Working with rasters allows the scale of the results to be adapted to the required purpose and does not have to be limited only to microbasins, but other units can also be taken into account, for example, functional areas of a spatial plan or urban blocks and districts. The study focuses on undeveloped areas; therefore, a unit capable of expressing the spatial division of the landscape was needed. The criteria for selecting this unit were as follows:

- variability of the units;
- potential of effective management.

Regarding the variability of the units, the aim was to avoid significant differences in the size of the units. When it comes to the functional areas of the spatial planning plan,

there are large differences between agricultural areas (on the order of hectares) and areas within communities (on the order of tens of meters). Although dividing into smaller areas allows for more precise identification of critical areas, it is not suitable for prioritizing areas. The potential of effective management and multifunctionality criteria lies in the ability to work effectively with measures to increase nature conservation. Natural retention focuses on the use of natural elements and ecosystems to retain and slow stormwater runoff and requires changes to measures within the catchment [77]. For an analysis of the retention functions, a section with a scale of at least 1:10,000 and a minimum pixel size of 5 × 5 m^2 is required [77].

In this article, a division of the area into 98 units is presented, representing individual microbasins resulting from the drainage conditions within the territory. Spatial plans in the Czech Republic are created at a scale of 1:5000 and require information with higher granularity. A division into the functional areas of a spatial plan is therefore an option. Within the AOI, there are 1016 areas with different types of use. In a more detailed breakdown, the analysis could be carried out at the level of individual plots, i.e., 8849 units (see Table 6 (Properties of different units) and Figure 14 (Evaluation of the spatial granularity of data using the example of pixels and microbasins)).

Table 6. Spatial characteristics of different units.

Type of Unit	N	Area [hectares] Min. Value	Area [hectares] Max	Area [hectares] Mean	Area [hectares] Median	Area [hectares] Standard Deviation	Area [hectares] Coefficient of Variation
Microbasins	98	3.854	61.11	24.80	22.94	11.96	0.48
Spatial plan units	1016	0.017	70.585	2.475	0.3855	7.63	3.08
Cadastral parcels	8849	0.017	47.537	0.284	0.066	1.25	4.39

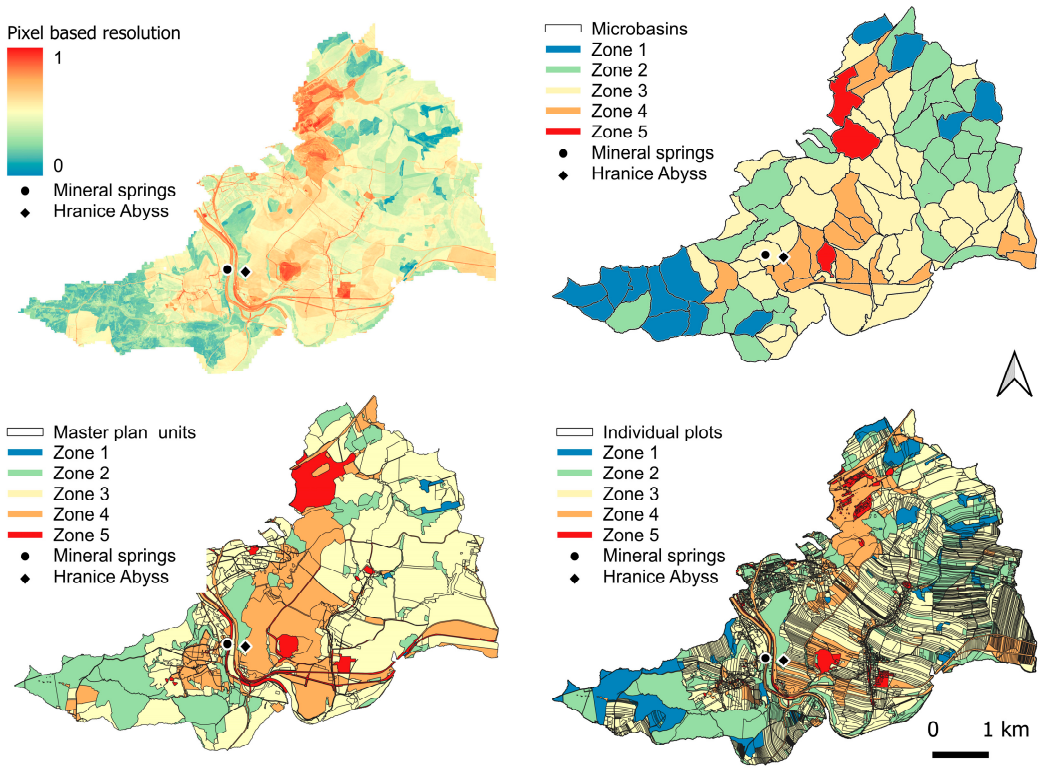


Figure 14. Examples of the spatial granularity of data in relation to spatial units.

5. Conclusions

This study introduces an innovative spatially explicit model that quantifies the secondary benefits of groundwater protection measures, focusing on increases in landscape retention capacity and changes in land surface temperature (LST). The model's key advancement lies in its use of high-resolution inputs (1×1 m), allowing for precise calculations of environmental impacts such as stormwater retention and LST reductions. This model is not only applicable to assess the externalities of groundwater protection measures but can also be used for the design of landscape greening, recreational areas, and erosion control measures, offering a versatile tool for various environmental management scenarios.

The development of this model enables the identification of priority zones for groundwater protection, precipitation infiltration, and surface temperature regulation. It allows for the assessment of targeted land-use changes based on accurate predictions of the environmental benefits associated with protective measures. The model deploys so-called adaptive capacity, which refers to the extent to which these measures are effective. Since each assessed unit—a microbasin—varies in land use, slopes, geological bedrock, and soils, its capacity to benefit from groundwater measures differs. The case study applies a common groundwater vulnerability measure, which involves converting intensive cropland to extensive grassland.

In the case study, the model demonstrated a significant increase in water retention capacity (up to 30%) with an average rise in precipitation retention of 18.2 mm per microbasin. In contrast, reductions in surface temperature were more modest, with a maximum decrease of 7.3%, corresponding to an average temperature drop of 1.5 °C. The study also revealed seasonal and land-use-specific variations in surface temperature, particularly in agricultural areas, where temperature fluctuations reached up to 2.6 °C between pre- and post-harvest periods.

The model is applied to a case study area comprising 98 microbasins and covering a total area of 25 km^2. A secondary goal is to determine in the case study area which microbasins the applied scenarios have the most significant effect, justifying the implemented measures. The results show the extent of measures differs significantly in their external effects—so-called adaptive capacity of applied measures—leading to the conclusion that each particular unit (in our case, a microbasin) must be evaluated individually due to its intrinsic characteristics, primarily due to differences in primary land use ratio, soil characteristics, and terrain configuration.

For instance, the adaptive capacity, i.e., the ability to improve a selected parameter based on land-use change, in Microbasin 1 (see Figure 12), where 90.2% of the land use is arable land, led to an increase in average retention capacity by 17.5 mm, or 25%. In the second microbasin, a similar improvement of 13.6 mm (an increase in capacity of 24.36%) was achieved by changing only 68.2% of the land use. In the third microbasin, the retention capacity increased by 16 mm (28%), but this required changing 93.5% of the area (from cropland to meadows). In these same microbasins, there was also a decrease in overall surface temperature: in the first microbasin by 1.53 °C, down to 23.67 °C; in the second by 1.33 °C, down to 23.84 °C; and in the third by 1.39 °C, down to 23.68 °C. This type of assessment provides data for spatially-based solutions.

The findings underscore the broader implications of land-use interventions, which not only protect groundwater resources but also enhance landscape resilience to climate change. This model offers critical insights into the environmental co-benefits of groundwater protection, establishing an essential tool for sustainable water resource management and climate-adaptive environmental planning.

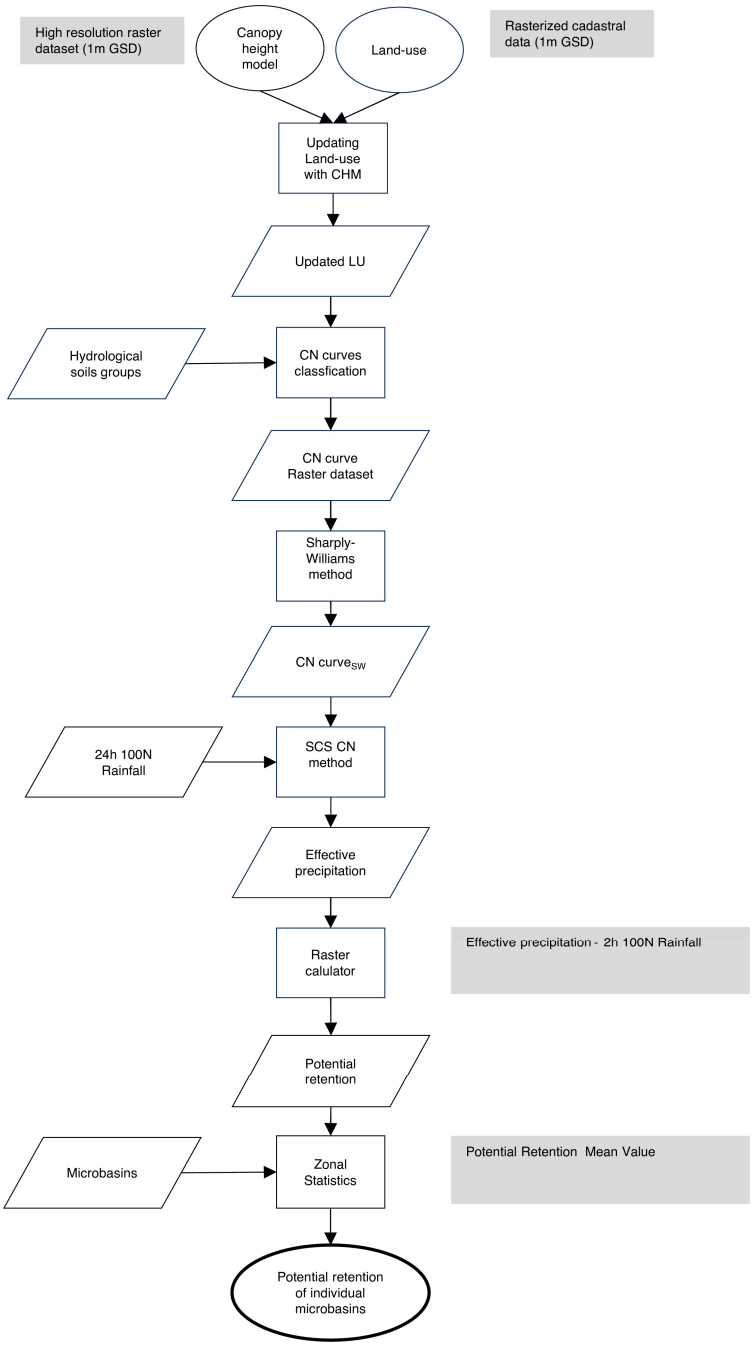
Author Contributions: Conceptualization, J.S. and P.K.; Writing—original draft, J.S.; Visualization, K.C. and J.S.; Investigation, J.S., K.C., O.U. and R.K.; Formal analysis, K.C. and O.U.; Writing—review and editing, H.V., K.K., P.O., V.V. and E.Ž.; Supervision, M.G., P.K. and V.V.; Funding acquisition, J.S. and J.Š.; Project Administration, J.S. and J.Š. All authors have read and agreed to the published version of the manuscript.

Funding: The research was financially supported by the Gregor Johann Mendel Grant Agency of the Mendel University in Brno, project Landscape in Whole and Landscape in Detail—an interdisciplinary research of the Hranice Karst.

Data Availability Statement: Data used for the research is available here: Spatially Explicit Model for Assessing the Impacts of Groundwater Protection Measures in the Vicinity of the Hranice Abyss. Raw Datasets for Spatially Explicit Model for Assessing the Impacts of Groundwater Protection Measures in the Vicinity of the Hranice Abyss. figshare. Dataset. https://doi.org/10.6084/m9.figshare.25075991.v1.

Conflicts of Interest: The authors declare no conflicts of interest. The funders had no role in the design of the study; in the collection, analyses, or interpretation of data; in the writing of the manuscript; or in the decision to publish the results.

Appendix A. Diagram of Retention Capacity Calculation Using the SCS CN Method Modified upon Sharply–Williams Applied in This Study



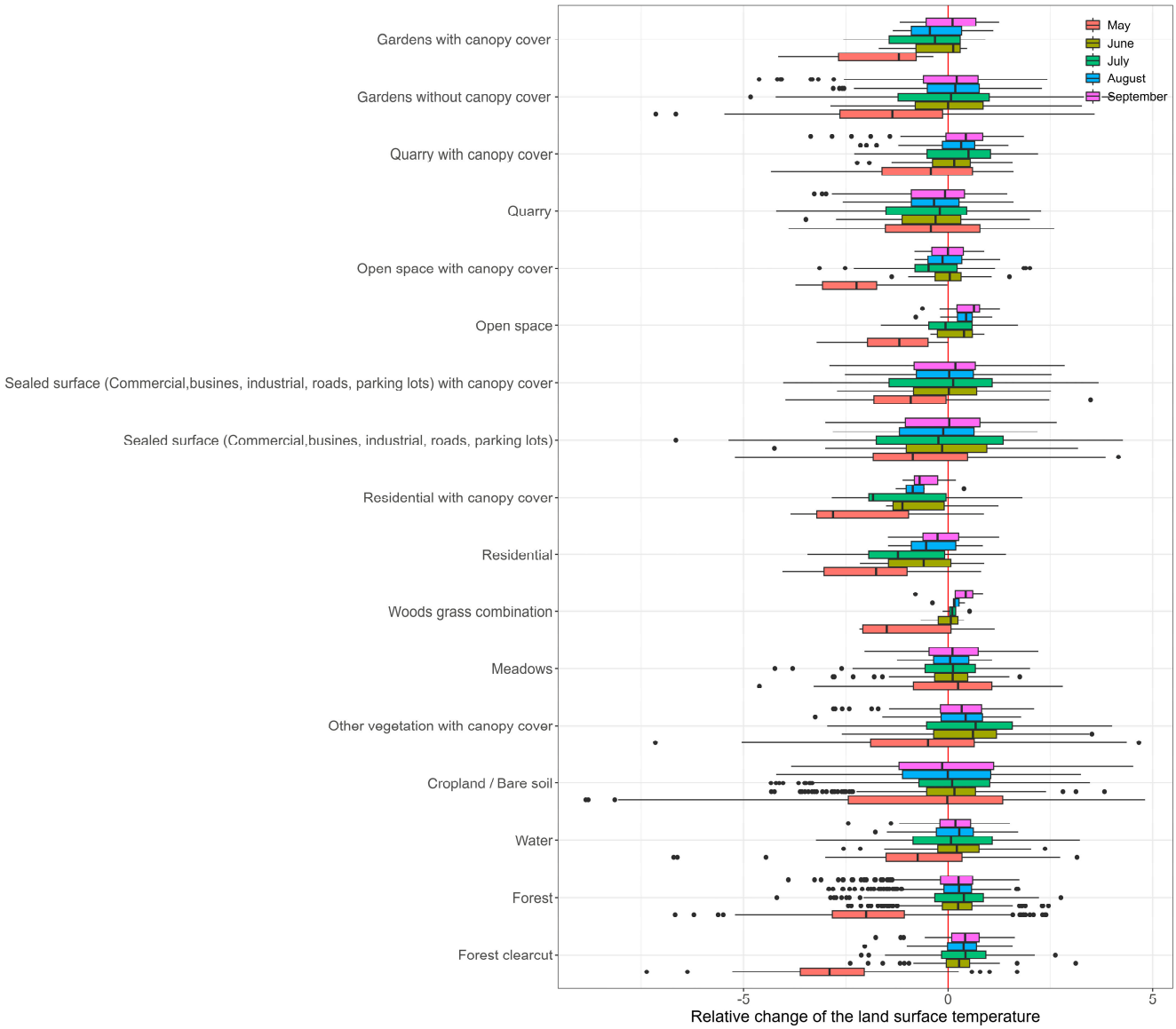
Appendix B. Convertor of Cadastral Units to LULC Categories

Cadastral Categories	LULC Categories	CHM Vegetation Type	LULC Categories with Vegetation
forest land	Forest	Low or Medium	Forest clearcut
forest land	Forest	High	Forest
water body	Water		Water
cropland	Cropland	None or Low	Cropland/Bare soil
cropland	Cropland	Medium or High	Other vegetation with canopy cover
permanent grassland	Grassland	None or Low	Meadows
permanent grassland	Grassland	Medium or High	Woods-grass combination
built-up residential area	Residential	None or Low or Medium	Residential
built-up residential area	Residential	High	Residential with canopy cover
built-up residential area, other area	Commercial, business, industrial, roads, parking lots (Sealed surface)	None or Low or Medium	Commercial, business, industrial, roads, parking lots (Sealed surface)
built-up residential area, other area	Sealed surface (Commercial, business, industrial, roads, parking lots) with canopy cover	High	Sealed surface (Commercial, business, industrial, roads, parking lots) with canopy cover
other area	Open space	None or Low or Medium	Open space
other area	Open space with canopy cover	High	Open space with canopy cover
Other area	Quarry	None or Low or Medium	Quarry
Other area	Quarry	High	Quarry with canopy cover
garden, orchard	Gardens without canopy cover	None or Low or Medium	Garden without canopy cover
garden, orchard	Gardens vegetation with canopy cover	High	Garden with canopy cover

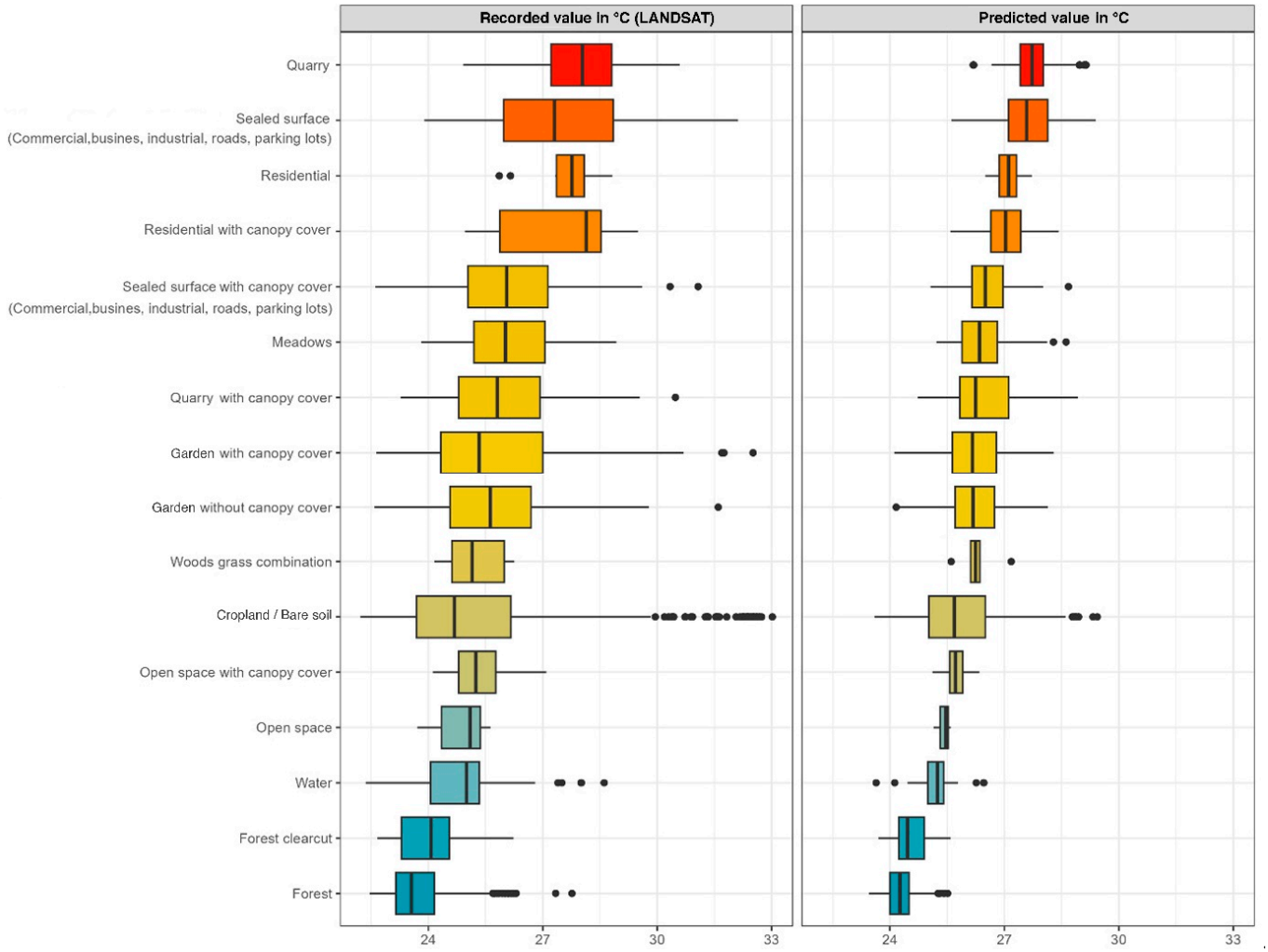
Appendix C. Table of Groundwater Samples with Descriptions of Concentrations and Detected Pollutants

No. of Locality	E—Exceeds Limits S—Sublimit Traces	Commentary
21-0006	E	The highest total concentration of pesticide metabolites in a single sample (2390.7 $ng \cdot L^{-1}$) was recorded at borehole HJ02. Additionally, the highest concentration of chloroacetamide pesticide metabolites (1050 $ng \cdot L^{-1}$ of metazachlor ESA) was also detected at this borehole.
21-0069	E	A very high total concentration of pesticide metabolites in a single sample (1744.9 $ng \cdot L^{-1}$) was recorded at the Černotín well, which is located within the built-up areas of the village Černotín. Additionally, a very high concentration of chloroacetamide pesticide metabolites (1400 $ng \cdot L^{-1}$ of metazachlor ESA) was also found in this well.
21-0038, 21-0039, 21-0066	E	Shallow wells (2.9–3.5 m in depth) located near each other in Teplice nad Bečvou were found to be contaminated by pharmaceuticals (diclofenac, ibuprofen) as well as pesticide metabolites, with concentrations reaching up to 1 $\mu g \cdot L^{-1}$. Trace concentrations of atrazine and its metabolites were also detected in these wells, despite atrazine being banned in the European Union since 2005 due to its environmental and health implications [39].
21-0001, 21-0002, 21-0003	T	Deep balneological boreholes in which trace concentrations of emerging organic contaminants (EOCs) were detected. For example, metazachlor ESA (63 $ng \cdot L^{-1}$) and metolachlor ESA (123 $ng \cdot L^{-1}$) were found in borehole 21-0001, diclofenac (47.4 $ng \cdot L^{-1}$) was detected in borehole 21-0003, and bisphenol A (125 $ng \cdot L^{-1}$) was identified in borehole R-I 21-0001.
21-0004, 21-0005, 21-0084, 21-0088	T	The samples originate from four lakes in various cave spaces within the Zbrašov Aragonite Caves. Trace amounts of atrazine and its metabolites were confirmed in all samples. Furthermore, trace amounts of chloridazon-DESPH, chloridazon-DESPH-ME, alachlor ESA, and the pharmaceutical diclofenac were detected. The presence of these compounds, even in trace amounts, suggests anthropogenic contamination within the karstic aquifer, underscoring the need for continued monitoring to assess environmental health and the potential risks associated with these residues [39].
21-0080, 21-0081, 21-0082, 21-0083, 21-0084	T	The samples, collected by divers, originate from the Hranice Abyss at depths of 20, 40, and 60 m. Noteworthy are the findings of trace concentration of EOC and CNm namely BPA (242 $ng \cdot L^{-1}$ in T-9), DEET (132 $ng \cdot L^{-1}$ in T-6), chloroacetanilide pesticides, and their metabolites (including alachlor ESA, metolachlor oxanilic acid (OA), metolachlor ESA, metazachlor OA, and metazachlor ESA), as well as compounds from the pyridazone group (chloridazon-DESPH, chloridazon-DESPH-ME) [39].
21-0050	E	The samples illustrate the high concentrations of pesticides and their metabolites present in the drainage waters near the Hranice Abyss, which have the potential to contaminate the thermal karst waters. Specifically, high concentrations of chloroacetamide pesticides and their metabolites (775 $ng \cdot L^{-1}$), as well as pyridazone group pesticides (686 $ng \cdot L^{-1}$), were measured.

Appendix D. Difference Between the Prediction Model and the Measured State



Appendix E. Comparison of the Prediction Model and the Measured State for the Sample from 22 June 2023



Notes

[1] Karst object layers are objects such as caves and sinkholes that are very well documented in a nationwide database or in JESO speleological archives [64] JESO.

[2] A possible karst object layer is a layer consisting of objects for which indicators such as terrain morphology (depressions) suggest that they may be sinkholes or limestone outcrops, which were documented by the author teams during the field investigation.

[3] Digital terrain model contains only the ground bare earth. It was created with the ANUDEM method from the LiDAR point cloud. Additionally, the lines of the watercourses were carved into the model, solid objects (buildings) were added, and drainless depressions were removed in order to make it hydrologically correct.

[4] Digital surface model captures both the natural and built/artificial features of the environment. Digital surface model was created from LiDAR point cloud.

References

1. Hollstein, L. Design with Nature Now, Edited by Frederick Steiner, Richard Weller, Karen M'Closkey, and Billy Fleming. *J. Urban Aff.* **2021**, *43*, 368–369. [CrossRef]
2. Moosavi, S.; Hurlimann, A.; Nielsen, J.; Bush, J.; Warren-Myers, G.; March, A. Transforming the Agency and Influence of Landscape Architects in Climate Change Actions: An Empirical Analysis of Barriers and Facilitators. *Landsc. Urban Plan.* **2023**, *234*, 104735. [CrossRef]
3. Council of Europe. European Landscape Convention. *Eur. Treaty Ser.* **2000**, *176*, 1–7.
4. Steinitz, C. *A Framework for Geodesign: Changing Geography by Design*; Esri: Redlands, CA, USA, 2012; ISBN 978-1-58948-333-0.

5. Liu, L.; Wu, J. Scenario Analysis in Urban Ecosystem Services Research: Progress, Prospects, and Implications for Urban Planning and Management. *Landsc. Urban Plan.* **2022**, *224*, 104433. [CrossRef]
6. IPBES. *Global Assessment Report on Biodiversity and Ecosystem Services of the Intergovernmental Science-Policy Platform on Biodiversity and Ecosystem Services*; Zenodo: Geneva, Switzerland, 2019.
7. Slätmo, E.; Nilsson, K.; Turunen, E. Implementing Green Infrastructure in Spatial Planning in Europe. *Land* **2019**, *8*, 62. [CrossRef]
8. Szitár, K.; Bánhidai, A.; Csecserits, A.; Csőszi, M.; Halassy, M.; Kertész, M.; Kollányi, L.; Schneller, K.; Teleki, M.; Vaszócsik, V.; et al. The Zone Cube Model—A Tool to Operationalise Green Infrastructure Prioritisation. *Landsc. Urban Plan.* **2024**, *243*, 104976. [CrossRef]
9. European Commission. REPORT FROM THE COMMISSION TO THE EUROPEAN PARLIAMENT AND THE COUNCIL THE MID-TERM REVIEW OF THE EU BIODIVERSITY STRATEGY TO 2020 The Mid-Term Review of the EU Biodiversity Strategy to 2020. 2015. Available online: https://eur-lex.europa.eu/legal-content/EN/TXT/?uri=CELEX:52015DC0478 (accessed on 1 October 2024).
10. Hansen, R.; Pauleit, S. From Multifunctionality to Multiple Ecosystem Services? A Conceptual Framework for Multifunctionality in Green Infrastructure Planning for Urban Areas. *Ambio* **2014**, *43*, 516–529. [CrossRef]
11. Kopperoinen, L.; Itkonen, P.; Niemelä, J. Using Expert Knowledge in Combining Green Infrastructure and Ecosystem Services in Land Use Planning: An Insight into a New Place-Based Methodology. *Landsc. Ecol.* **2014**, *29*, 1361–1375. [CrossRef]
12. Chatzimentor, A.; Apostolopoulou, E.; Mazaris, A.D. A Review of Green Infrastructure Research in Europe: Challenges and Opportunities. *Landsc. Urban Plan.* **2020**, *198*, 103775. [CrossRef]
13. Wellmann, T.; Lausch, A.; Andersson, E.; Knapp, S.; Cortinovis, C.; Jache, J.; Scheuer, S.; Kremer, P.; Mascarenhas, A.; Kraemer, R.; et al. Remote Sensing in Urban Planning: Contributions towards Ecologically Sound Policies? *Landsc. Urban Plan.* **2020**, *204*, 103921. [CrossRef]
14. Choi, C.; Berry, P.; Smith, A. The Climate Benefits, Co-Benefits, and Trade-Offs of Green Infrastructure: A Systematic Literature Review. *J. Environ. Manag.* **2021**, *291*, 112583. [CrossRef] [PubMed]
15. Zhang, K.; Chui, T.F.M. Linking Hydrological and Bioecological Benefits of Green Infrastructures across Spatial Scales—A Literature Review. *Sci. Total Environ.* **2019**, *646*, 1219–1231. [CrossRef] [PubMed]
16. O'Brien, L.; De Vreese, R.; Kern, M.; Sievänen, T.; Stojanova, B.; Atmiş, E. Cultural Ecosystem Benefits of Urban and Peri-Urban Green Infrastructure across Different European Countries. *Urban For. Urban Green.* **2017**, *24*, 236–248. [CrossRef]
17. Korkou, M.; Tarigan, A.K.M.; Hanslin, H.M. The Multifunctionality Concept in Urban Green Infrastructure Planning: A Systematic Literature Review. *Urban For. Urban Green.* **2023**, *85*, 127975. [CrossRef]
18. Benedict, M.A.; MacMahon, E.T. Green Infrastructure: Smart Conservation for the 21st Century. *Renew. Resour. J.* **2002**, *20*, 12–17.
19. Brillinger, M.; Scheuer, S.; Albert, C. Deliberating Options for Nature-Based River Development: Insights from a Participatory Multi-Criteria Evaluation. *J. Environ. Manag.* **2022**, *317*, 115350. [CrossRef]
20. Koutsovili, E.I.; Tzoraki, O.; Kalli, A.A.; Provatas, S.; Gaganis, P. Participatory Approaches for Planning Nature-Based Solutions in Flood Vulnerable Landscapes. *Environ. Sci. Policy* **2023**, *140*, 12–23. [CrossRef]
21. Coletta, V.R.; Pagano, A.; Pluchinotta, I.; Fratino, U.; Scrieciu, A.; Nanu, F.; Giordano, R. Causal Loop Diagrams for Supporting Nature Based Solutions Participatory Design and Performance Assessment. *J. Environ. Manag.* **2021**, *280*, 111668. [CrossRef]
22. Neuhoff, R.; Simeone, L.; Laursen, L.H. Forms of Participatory Futuring for Urban Sustainability: A Systematic Review. *Futures* **2023**, *154*, 103268. [CrossRef]
23. Finch, T.; Bradbury, R.B.; Bradfer-Lawrence, T.; Buchanan, G.M.; Copping, J.P.; Massimino, D.; Smith, P.; Peach, W.J.; Field, R.H. Spatially Targeted Nature-Based Solutions Can Mitigate Climate Change and Nature Loss but Require a Systems Approach. *One Earth* **2023**, *6*, 1350–1374. [CrossRef]
24. Al Khoury, I.; Boithias, L.; Bailey, R.T.; Ollivier, C.; Sivelle, V.; Labat, D. Impact of Land-Use Change on Karst Spring Response by Integration of Surface Processes in Karst Hydrology: The ISPEEKH Model. *J. Hydrol.* **2023**, *626*, 130300. [CrossRef]
25. Mahmoud, M.; Liu, Y.; Hartmann, H.; Stewart, S.; Wagener, T.; Semmens, D.; Stewart, R.; Gupta, H.; Dominguez, D.; Dominguez, F.; et al. A Formal Framework for Scenario Development in Support of Environmental Decision-Making. *Environ. Model. Softw.* **2009**, *24*, 798–808. [CrossRef]
26. Wu, J.; Xia, L.; On Chan, T.; Awange, J.; Zhong, B. Downscaling Land Surface Temperature: A Framework Based on Geographically and Temporally Neural Network Weighted Autoregressive Model with Spatio-Temporal Fused Scaling Factors. *ISPRS J. Photogramm. Remote Sens.* **2022**, *187*, 259–272. [CrossRef]
27. Van Oijstaeijen, W.; Silva, M.F.e.; Back, P.; Collins, A.; Verheyen, K.; De Beelde, R.; Cools, J.; Van Passel, S. The Nature Smart Cities Business Model: A Rapid Decision-Support and Scenario Analysis Tool to Reveal the Multi-Benefits of Green Infrastructure Investments. *Urban For. Urban Green.* **2023**, *84*, 127923. [CrossRef]
28. Miller, J.D.; Vesuviano, G.; Wallbank, J.R.; Fletcher, D.H.; Jones, L. Hydrological Assessment of Urban Nature-Based Solutions for Urban Planning Using Ecosystem Service Toolkit Applications. *Landsc. Urban Plan.* **2023**, *234*, 104737. [CrossRef]
29. Ravbar, N.; Pipan, T. Karst Groundwater Dependent Ecosystems—Typology, Vulnerability and Protection. In *Encyclopedia of Inland Waters*, 2nd ed.; Mehner, T., Tockner, K., Eds.; Elsevier: Oxford, UK, 2022; pp. 460–473. ISBN 978-0-12-822041-2.
30. Xiong, L.; Li, R. Assessing and Decoupling Ecosystem Services Evolution in Karst Areas: A Multi-Model Approach to Support Land Management Decision-Making. *J. Environ. Manag.* **2024**, *350*, 119632. [CrossRef]

31. Sedláček, J.; Šimečková, J.; Geršl, M.; Kučera, P.; Vavrouchová, H.; Vlček, V.; Chaloupský, P.; Klepárník, R.; Ulrich, O.; Kohoutková, K. *Krajina v Celku a Krajina v Detailu Mezioborový Výzkum Hranického Krasu*, 1st ed.; Mendelova Univerzita v Brně: Brno, Czech Republic, 2023; ISBN 978-80-7509-935-8.
32. European Commision. Environmental Impact Assessment—Environment—European Commission. Available online: http://ec.europa.eu/environment/eia/index_en.htm (accessed on 25 July 2016).
33. *Communication from the Commission to the European Parliament, the European Council, the Council, the European Economic and Social Committee and the Committee of the Regions the European Green Deal*; European Commission: Brussels, Belgium, 2019.
34. Hoek, N. A Critical Analysis of the Proposed EU Regulation on Nature Restoration: Have the Problems Been Resolved? *Eur. Energy Environ. Law Rev.* **2022**, *31*, 320–333. [CrossRef]
35. QGIS.org, 3.28 2023 (Software). QGIS Geographic Information System. QGIS Association. Available online: http://www.qgis.org (accessed on 1 October 2024).
36. van Oorschot, J.; Sprecher, B.; van 't Zelfde, M.; van Bodegom, P.M.; van Oudenhoven, A.P.E. Assessing Urban Ecosystem Services in Support of Spatial Planning in the Hague, the Netherlands. *Landsc. Urban Plan.* **2021**, *214*, 104195. [CrossRef]
37. *Protected Zones of Water Sources and Spa Locations*; Ministry of Health of Czech Republic, Praha: Praha, Czech Republic, 2015.
38. Oppeltová, P.; Vlček, V.; Geršl, M.; Chaloupský, P.; Ulrich, O.; Sedláček, J.; Vavrouchová, H.; Kohoutková, K.; Klepárník, R.; Šimečková, J. Occurrence and Path Pollution of Emerging Organic Contaminants in Mineral Water of Hranice Hypogenic Karst. *Front. Environ. Sci.* **2024**, *12*, 1339818. [CrossRef]
39. Sracek, O.; Geršl, M.; Faimon, J.; Bábek, O. The Geochemistry and Origin of Fluids in the Carbonate Structure of the Hranice Karst with the World's Deepest Flooded Cave of the Hranicka Abyss, Czech Republic. *Appl. Geochem.* **2019**, *100*, 203–212. [CrossRef]
40. Foster, S. Fundamental Concepts in Aquifer Vulnerability, Pollution Risk and Protection Strategy. In Proceedings of the Vulnerability of Soil and Groundwater to Pollutants, International Conference, Noordwijk aan Zee, The Netherlands, 30 March 1987.
41. Moreno-Gómez, M.; Liedl, R.; Stefan, C.; Pacheco, J. Theoretical Analysis and Considerations of the Main Parameters Used to Evaluate Intrinsic Karst Groundwater Vulnerability to Surface Pollution. *Sci. Total Environ.* **2024**, *907*, 167947. [CrossRef] [PubMed]
42. Zwahlen, F. *Vulnerability and Risk Mapping for the Protection of Carbonate (Karst) Aquifers*; Office for Official Publications of the European Communities: Luxembourg, 2003.
43. Li, Y.; Li, M.; Song, X.; Hu, X.; Guo, X.; Qiu, Y.; Xiong, H.; Cui, H.; Ma, C. An Integrated Approach Combining LISA, BI-LISA, and the Modified COPK Method to Improve Groundwater Management in Large-Scale Karst Areas. *J. Hydrol.* **2023**, *625*, 130111. [CrossRef]
44. Masson-Delmotte, V.; Zhai, P.; Pirani, A.; Connors, S.L.; Péan, C.; Berger, S.; Zhou, B. (Eds.) *Climate Change 2021: The Physical Science Basis. Contribution of Working Group I to the Sixth Assessment Report of the Intergovernmental Panel on Climate Change*; Cambridge University Press: Cambridge, UK, 2021.
45. European Environment Agency. *European Climate Risk Assessment*; European Environment Agency: Copenhagen, Denmark, 2024.
46. Zeder, J.; Fischer, E.M. Observed Extreme Precipitation Trends and Scaling in Central Europe. *Weather Clim. Extrem.* **2020**, *29*, 100266. [CrossRef]
47. Feldman, A. *Hydrologic Modeling System HEC-HMS: Technical Reference Manual*; US Army Corps of Engineers, Institute for Water Resources, Hydrologic Engineering Center: Davis, UT, USA, 2000.
48. Akbari, A.; Abu Samah, A.; Ngien, S. Effect of Slope Adjustment on Curve Number Using Global Digital Elevation Data: New Look into Sharply-Williams and Huang Methods. In Proceedings of the Second International Conference on Science, Engineering & Environment, Osaka, Japan, 21–23 November 2016.
49. Janeček, M.; Dostál, T.; Kozlovsky-Dufková, J.; Dumbrovský, M.; Hůla, J.; Kadlec, V.; Konečná, J.; Kovář, P.; Krása, J.; Kubátová, E.; et al. Ochrana Zemědělské Půdy Před Erozí. *Metodika* **2012**, *113*.
50. Kovář, P.; Heřmanovská, D.; Sůva, M. DES RAIN 2015. Available online: https://www.fzp.czu.cz/dl/42056?lang=cs (accessed on 1 October 2024).
51. *Climate Resilience Policy Indicator*; International Energy Agency: Zlin, Czech Republic, 2023. Available online: https://www.iea.org/articles/czech-republic-climate-resilience-policy-indicator (accessed on 1 October 2024).
52. Stewart, I.D. A Systematic Review and Scientific Critique of Methodology in Modern Urban Heat Island Literature. *Int. J. Climatol.* **2011**, *31*, 200–217. [CrossRef]
53. Seiner, J. *Landschaftspark Neckar 2008. Change to: Baumgärtner, C. Der Regionale Landschaftspark*, 1st ed.; Schriftenreihe Stadt und Landschaft; Städtebau-Institut der Universität Stuttgart: Stuttgart, Germany, 2015; ISBN 978-3-939486-96-1.
54. Schwab, A. Regionale Klimaanalyse Donau-Iller 2015. Available online: https://www.google.com/url?sa=t&source=web&rct=j&opi=89978449&url=https://www.rvdi.de/fileadmin/regionalentwicklung/umwelt/Regionale_Klimaanalyse_Abschlussbericht_red.pdf&ved=2ahUKEwiX-vigiJCJAxV7h_0HHZ66ECAQFnoECBYQAQ&usg=AOvVaw1vWeTPzas1MZzTO9NjOGD6 (accessed on 1 October 2024).
55. USGS. Earth Explorer. Available online: https://earthexplorer.usgs.gov/ (accessed on 4 September 2023).
56. Breiman, L. Random Forests. *Mach. Learn.* **2001**, *45*, 5–32. [CrossRef]
57. Hutengs, C.; Vohland, M. Downscaling Land Surface Temperatures at Regional Scales with Random Forest Regression. *Remote Sens. Environ.* **2016**, *178*, 127–141. [CrossRef]

58. Špaček, P.; Bábek, O.; Štěpančíková, P.; Švancara, J.; Pazdírková, J.; Sedláček, J. The Nysa-Morava Zone: An Active Tectonic Domain with Late Cenozoic Sedimentary Grabens in the Western Carpathians' Foreland (NE Bohemian Massif). *Int. J. Earth Sci.* **2015**, *104*, 963–990. [CrossRef]
59. Vysoká, H.; Bruthans, J.; Falteisek, L.; Žák, K.; Rukavičková, L.; Holeček, J.; Schweigstillová, J.; Oster, H. Hydrogeology of the Deepest Underwater Cave in the World: Hranice Abyss, Czechia. *Hydrogeol. J.* **2019**, *27*, 2325–2345. [CrossRef]
60. ESRI 2011. *ArcGIS Pro: Release 3.0.2*; Environmental Systems Research Institute: Redlands, CA, USA, 2011. Available online: http://www.rstudio.com/ (accessed on 1 October 2024).
61. RStudio Team. *RStudio: Integrated Development for R. RStudio*; PBC: Boston, MA, USA, 2022.
62. Hutchinson, M.F. A New Procedure for Gridding Elevation and Stream Line Data with Automatic Removal of Spurious Pits. *J. Hydrol.* **1989**, *106*, 211–232. [CrossRef]
63. LAS Specification 1.4—R14 2018. Available online: https://www.asprs.org/wp-content/uploads/2019/03/LAS_1_4_r14.pdf (accessed on 28 January 2024).
64. AOPK, N.C.A. of the Czech Republic. Unified Database of Speleological Objects (JESO) 2023. Available online: https://jeso.nature.cz/ (accessed on 1 October 2024).
65. ČÚZK National Open Data Catalog 2023. Available online: https://cuzk.gov.cz/en (accessed on 1 September 2023).
66. Halešová, T.; Kotyzová, M. Grassing of Zone I in the Moravian Karst Protected Landscape Area. *Nat. Conserv. J.* **2022**, 40–43.
67. Bartesaghi-Koc, C.; Osmond, P.; Peters, A. Quantifying the Seasonal Cooling Capacity of 'Green Infrastructure Types' (GITs): An Approach to Assess and Mitigate Surface Urban Heat Island in Sydney, Australia. *Landsc. Urban Plan.* **2020**, *203*, 103893. [CrossRef]
68. Wei, B.; Li, Z.; Duan, L.; Gu, Z.; Liu, X. Vegetation Types and Rainfall Regimes Impact on Surface Runoff and Soil Erosion over 10 Years in Karst Hillslopes. *CATENA* **2023**, *232*, 107443. [CrossRef]
69. Xiao, R.; Wang, G.; Zhang, Q.; Zhang, Z. Multi-Scale Analysis of Relationship between Landscape Pattern and Urban River Water Quality in Different Seasons. *Sci. Rep.* **2016**, *6*, 25250. [CrossRef] [PubMed]
70. Madureira, H.; Andresen, T. Planning for Multifunctional Urban Green Infrastructures: Promises and Challenges. *Urban Des. Int.* **2014**, *19*, 38–49. [CrossRef]
71. Meerow, S.; Newell, J.P. Spatial Planning for Multifunctional Green Infrastructure: Growing Resilience in Detroit. *Landsc. Urban Plan.* **2017**, *159*, 62–75. [CrossRef]
72. Mozny, M.; Hajkova, L.; Vlach, V.; Ouskova, V.; Musilova, A. Changing Climatic Conditions in Czechia Require Adaptation Measures in Agriculture. *Climate* **2023**, *11*, 210. [CrossRef]
73. World Bank Open Data World Bank Open Data. Available online: https://data.worldbank.org/indicator/SP.RUR.TOTL.ZS?locations=CZ (accessed on 25 January 2024).
74. Křištofová, K.; Lehnert, M.; Martinát, S.; Tokar, V.; Opravil, Z. Adaptation to Climate Change in the Eastern Regions of the Czech Republic: An Analysis of the Measures Proposed by Local Governments. *Land Use Policy* **2022**, *114*, 105949. [CrossRef]
75. Šilhánková, V.; Pondělíček, M.; Černá, E.; Emmer, A.; HubatovÃ, M. The Perception of Risks Caused by Climate Change in the Urban Environment by the City Population and Its Usefulness in Identifying Measures for Alleviating Their Impacts. *WSEAS Trans. Environ. Dev.* **2016**, *12*, 9–19.
76. Sandin, P. Better Safe Than Sorry: Applying Philosophical Methods to the Debate on Risk and the Precautionary Principle. Ph.D. Thesis, Royal Institute of Technology, Stockholm, Sweden, 2004.
77. Pechanec, V.; Cudlín, P.; Machar, I.; Brus, J.; Kiliánová, H. Modelling of the Water Retention Capacity of the Landscape. In *Assessment and Protection of Water Resources in the Czech Republic*; Springer Water: Cham, Siwtzerland, 2020; ISBN 978-3-030-18362-2.

Disclaimer/Publisher's Note: The statements, opinions and data contained in all publications are solely those of the individual author(s) and contributor(s) and not of MDPI and/or the editor(s). MDPI and/or the editor(s) disclaim responsibility for any injury to people or property resulting from any ideas, methods, instructions or products referred to in the content.